Assessing El Niño Southern Oscillation variability during the past millennium

D. Khider,[1] L. D. Stott,[1] J. Emile-Geay,[1] R. Thunell,[2] and D. E. Hammond[1]

[1]   We present a reconstruction of El Niño Southern Oscillation (ENSO) variability spanning the Medieval Climate Anomaly (MCA, A.D. 800–1300) and the Little Ice Age (LIA, A.D. 1500–1850). Changes in ENSO are estimated by comparing the spread and symmetry of $\delta^{18}O$ values of individual specimens of the thermocline-dwelling planktonic foraminifer *Pulleniatina obliquiloculata* extracted from discrete time horizons of a sediment core collected in the Sulawesi Sea, at the edge of the western tropical Pacific warm pool. The spread of individual $\delta^{18}O$ values is interpreted to be a measure of the strength of both phases of ENSO while the symmetry of the $\delta^{18}O$ distributions is used to evaluate the relative strength/frequency of El Niño and La Niña events. In contrast to previous studies, we use robust and resistant statistics to quantify the spread and symmetry of the $\delta^{18}O$ distributions; an approach motivated by the relatively small sample size and the presence of outliers. Furthermore, we use a pseudo-proxy approach to investigate the effects of the different paleo-environmental factors on the statistics of the $\delta^{18}O$ distributions, which could bias the paleo-ENSO reconstruction. We find no systematic difference in the magnitude/strength of ENSO during the Northern Hemisphere MCA or LIA. However, our results suggest that ENSO during the MCA was skewed toward stronger/more frequent La Niña than El Niño, an observation consistent with the medieval megadroughts documented from sites in western North America.

Citation: Khider, D., L. D. Stott, J. Emile-Geay, R. Thunell, and D. E. Hammond (2011), Assessing El Niño Southern Oscillation variability during the past millennium, *Paleoceanography*, *26*, PA3222, doi:10.1029/2011PA002139.

1.   Introduction

[2]   The El Niño Southern Oscillation (ENSO), centered in the tropical Pacific Ocean, is the leading mode of interannual climate variability in the global climate system. Because of its influence on weather patterns and its associated socio-economic impacts, growing concern about potential changes in ENSO strength and/or frequency in response to future sea surface warming in the tropics have made its study (and, if possible, its prediction) a priority. Climate models that are forced with increased greenhouse gas concentrations simulate changes in ENSO variability but importantly, the models do not agree on the sign of change nor on the mean state of the tropical Pacific Ocean [*Meehl et al.*, 2007]. Therefore, paleoclimate records that are able to document past ENSO variability provide a useful reference against which to test models that attempt to simulate the natural behavior of ENSO. However, studies of past ENSO variability have been hampered by a lack of long, continuous, and annually resolved paleoclimatic archives from the equatorial Pacific. Much of our current understanding of past ENSO variability has been obtained from geochemical data derived from corals [i.e., *Cobb et al.*, 2003; *Dunbar et al.*, 1994; *Quinn et al.*, 2006]. The geochemistry of coral skeletons documents hydrographic conditions from the center of action of ENSO; however, most existing coral records span only the last 200 years, limiting their usefulness as long-term recorders of ENSO [*Jones and Mann*, 2004]. Longer ENSO reconstructions can be obtained from high-resolution terrestrial archives located outside the tropical Pacific Ocean [*Anderson*, 1992; *Moy et al.*, 2002; *Quinn*, 1992; *Thompson et al.*, 1984]. These proxies rely on the assumption that the sign and the strength of the teleconnection with ENSO has remained constant over time; a hypothesis that has yet to be thoroughly tested.

[3]   Over the past few decades, a variety of proxies have been used to investigate the behavior of ENSO during the Little Ice Age (LIA, defined here as the period between A.D. 1500 and 1850) and the Medieval Climate Anomaly (MCA, A.D. 800 to 1300). The results from these studies paint a very complex and, at times, contradictory picture of ENSO behavior during the past millennium (see, for example, *Cobb et al.* [2003] and *Conroy et al.* [2009] versus *Conroy et al.* [2008] and *Moy et al.* [2002] or *Cobb et al.* [2003] versus *Hereid et al.* [2009]). This complexity underscores the need for additional high-resolution proxy records from within the tropical Pacific Ocean capable of recording ENSO variability over long time scales. Furthermore, recent

[1]Department of Earth Sciences, University of Southern California, Los Angeles, California, USA.
[2]Department of Earth and Ocean Sciences, University of South Carolina, Columbia, South Carolina, USA.
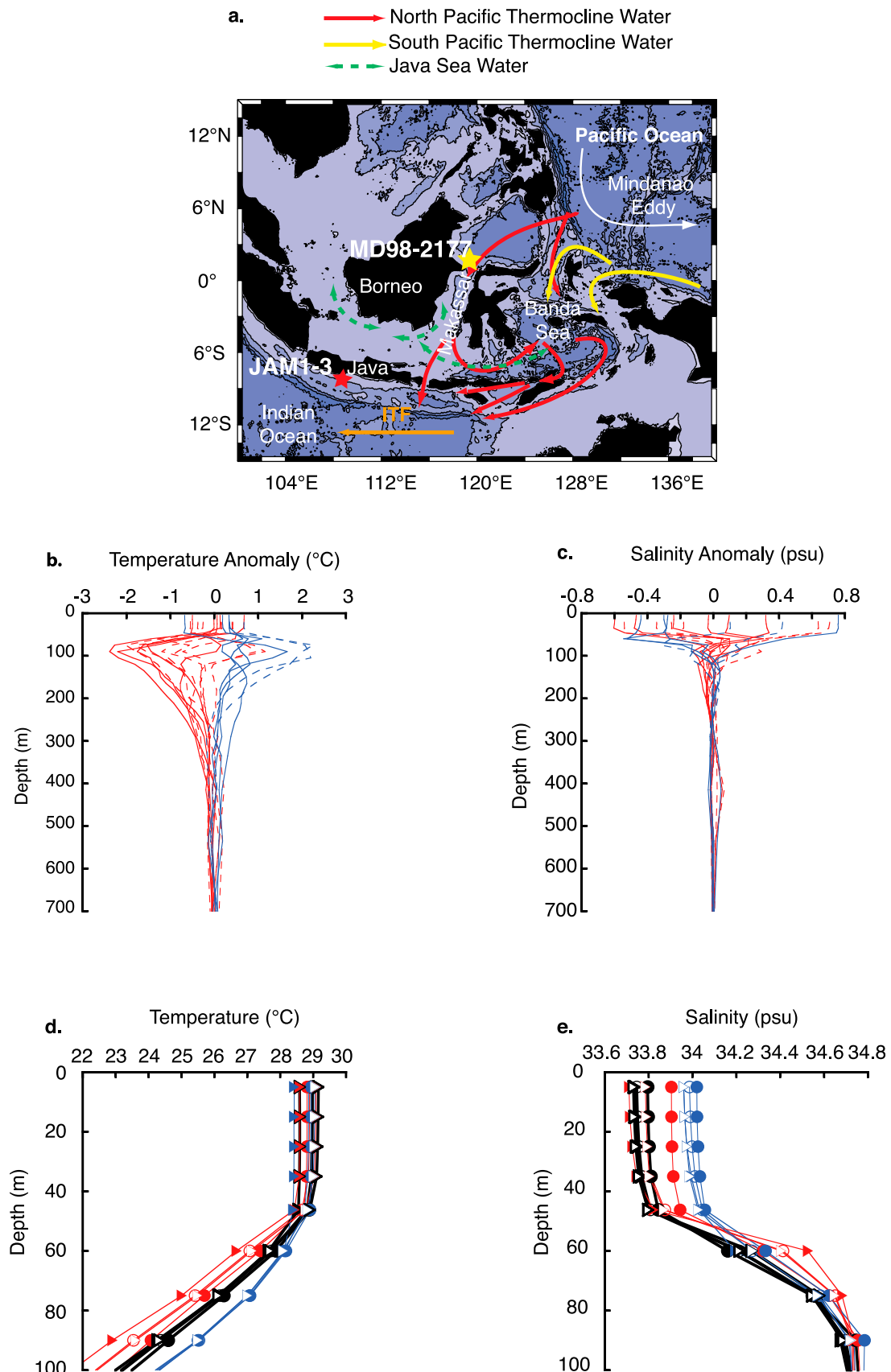
a.

→ North Pacific Thermocline Water
→ South Pacific Thermocline Water
- - → Java Sea Water

Figure 1

observations have identified two apparent "flavors" of ENSO [i.e., *Trenberth and Stepaniak*, 2001], each characterized by a different spatial pattern of sea surface temperature (SST) anomalies in the tropical Pacific and each having distinct extratropical teleconnection patterns [i.e., *Ashok et al.*, 2007; *Kumar et al.*, 2006]. These observations further emphasize the need to expand the network of high-resolution proxy records from the central and western tropical Pacific Ocean.

[4] Marine sediment cores can provide long and continuous archives of ocean conditions within the tropics that contain information about ENSO variability. For instance, core MD98-2177 (hereafter MD77), collected from the northern entrance of the Makassar Strait in the Indo-Pacific warm pool (Figure 1), is suitably located to study past changes in ENSO behavior because the thermocline temperatures at this site are highly correlated with ENSO [*Ffield et al.*, 2000, Figure 1 and Section 2]. However, MD77, like most marine sediment cores, cannot provide discrete, annually resolved samples because sedimentation rates are too low and the sediments are bioturbated. We present a method for extracting ENSO history from samples taken from the MD77 core that overcomes the lack of annual resolution. The method involves the measurements of the oxygen isotopic composition (δ^{18}O) of individual shells of the planktonic foraminifer *Pulleniatina obliquiloculata* that calcifies within the tropical thermocline. Since planktonic foraminifera secrete a calcite shell on a timescale of 2–4 weeks [*Spero*, 1998], the stable isotope composition of individual foraminiferal tests of a large population of specimens can provide an estimate of the spectrum of monthly surface to sub-surface temperature and salinity changes that accompany the seasonal cycle and interannual variability [*Stott and Tang*, 1996; *Tang and Stott*, 1993], including ENSO [*Koutavas et al.*, 2006; *Leduc et al.*, 2009] over the range of calcification depths that apply to *P. obliquiloculata*. In section 3, we introduce a conceptual model to explore the relative impact of these parameters on the δ^{18}O distributions obtained from individual *P. obliquiloculata*. From this pseudo-proxy model, we demonstrate that changes in the spread and symmetry of these distributions are attributable to ENSO variability. Specifically, an increase in the strength and frequency of both El Niño and La Niña events will result in an overall increase in the spread of the individual δ^{18}O values within a sample while a change in the relative strength of either El Niño or La Niña events will impart a skewness to the distributions [*Koutavas et al.*, 2006; *Leduc et al.*, 2009]. For this study, we sampled MD77 at discrete horizons that correspond to the MCA and LIA sections of the core and analyzed ~70 individual specimens of

P. obliquiloculata at each horizon, resulting in 'snapshots' of ENSO variability over the past millennium.

2. Oceanographic Settings

2.1. El Niño and the Southern Oscillation in the Western Tropical Pacific

[5] ENSO is an interannual mode of climate variability associated with a disturbance of the Walker circulation over the tropical Pacific Ocean [*Rasmusson and Carpenter*, 1982]. Over the late 20th century, observations from the tropical Pacific have shown that at 2–7 year intervals, the easterly trade winds relax, and this allows the pool of warm western Pacific surface waters to migrate toward the central and eastern tropical Pacific. As these warm surface waters shift eastward during an El Niño, so does the zone of strong atmospheric convection. The sea surface temperature anomalies associated with El Niño disrupt atmospheric circulation within the Hadley cell and in doing so, influence weather systems globally. As wind stress decreases over the eastern tropical Pacific during an El Niño, the strength of upwelling also decreases and hence, the thermocline deepens across the central and eastern tropical Pacific. In the western Pacific, the subsurface response is just the opposite: the thermocline shoals during an El Niño. In contrast to El Niño, La Niña conditions are characterized by intensified trade winds, warmer surface conditions than usual, and a deepening of the thermocline in the western tropical Pacific. The atmosphere responds to these oceanic conditions with a seesaw pattern in sea level pressure anomalies between Tahiti and Darwin (Australia), which is referred to as the Southern Oscillation. Thus, the coupled ocean-atmosphere process has been termed the El Niño Southern Oscillation (ENSO).

[6] Two different flavors of "El Niño" [*Trenberth and Stepaniak*, 2001] have been identified, based on the location of the maximum positive SST anomalies. Although there are differences among studies that attempt to characterize these different modes of ENSO [i.e., *Ashok et al.*, 2007; *Kug et al.*, 2009; *Kumar et al.*, 2006; *Larkin and Harrison*, 2005a, 2005b; *Trenberth and Stepaniak*, 2001], the cold tongue El Niño (thereafter, EP El Niño), similar to the canonical El Niño described by *Rasmusson and Carpenter* [1982], exhibits a maximum sea surface warming in the eastern Pacific. In contrast, some events show positive SST anomalies mostly confined to the Niño 4 region. These El Niños have been referred to as "dateline El Niño" [*Larkin and Harrison*, 2005a], "central Pacific (CP) El Niño" [*Kao and Yu*, 2009], "warm pool El Niño" [*Kug et al.*, 2009], or "El Niño Modoki" [*Ashok and Yamagata*, 2009; *Ashok et al.*, 2007]. This central

Figure 1. (a) Schematic of the ITF and related currents in the Indonesian Seas adapted from *Gordon* [2005]. The location of core MD98-2177 is shown in yellow. The location of the sediment trap study by *Mohtadi et al.* [2009] is represented in red. (b) Annual temperature anomalies associated with ENSO dynamics at the MD98-2177 location obtained from the EMCWF ORA-S3 reanalysis. (c) Annual salinity anomalies associated with ENSO dynamics. A year was defined from May of year 1 to April of year 2 to accentuate the seasonal locking of the ENSO cycle. Moderate to strong events were selected based on the consensus list of El Niño and La Niña years (http://ggweather.com/enso/oni.htm). El Niño (La Niña) events are represented in red (blue). EP ENSO events are represented by a solid line while CP ENSO events are represented by a dashed line. (d) Mean annual (open circle), summer (JAS, filled circle), and winter (DJF, filled triangle) temperature during El Niño (red), La Niña (blue), and normal years (black). (e) Mean annual (open circle), summer (JAS, filled circle), and winter (DJF, filled triangle) salinity during El Niño (red), La Niña (blue), and normal years (black).

Pacific warming may be accompanied by a weak cold tongue warming [*Kug et al.*, 2009] or cooling [*Ashok and Yamagata*, 2009; *Ashok et al.*, 2007; *Yeh et al.*, 2009]. Both events are characterized by cooler surface waters than normal in the western tropical Pacific. CP El Niño has occurred more frequently since 1976 in association with a weakening of the easterly trade winds and a flattening of the equatorial thermocline gradient [*Ashok et al.*, 2007; *Yeh et al.*, 2009]. Conversely, CP La Niña is characterized by large negative SST anomalies in the central equatorial Pacific flanked on both sides by positive SST anomalies [*Ashok and Yamagata*, 2009]. Furthermore, the EP type of ENSO tends to produce strong El Niño events but relatively weak La Niña events. A reverse tendency has been shown for CP ENSO events [*Kao and Yu*, 2009].

[7] The mechanisms leading to the CP ENSO are not well understood. Recently, *Yu et al.* [2011] demonstrated that some ENSO events are actually of both types. For instance, the 1982/83 El Niño was a weak CP event followed by a strong EP event. On the other hand, *Ashok et al.* [2007] suggested that CP El Niño is not part of the traditional El Niño evolution and that these two types of ENSO behavior are fundamentally different phenomena, especially after the 1970s. Indeed, the transition mechanism and dynamical subsurface structure of a CP El Niño is inconsistent with the traditional delayed oscillator/discharge concept [*Kao and Yu*, 2009; *Kug et al.*, 2009] and so is the pattern, amplitude, and even sign of the extratropical atmospheric teleconnections associated with these two types of ENSO [i.e., *Ashok et al.*, 2007; *Larkin and Harrison*, 2005a]. For instance, changes in the extent and location of tropical Pacific warming have been shown to alter the teleconnection with rainfall and temperature anomalies over Asia, North America and Australia [*Ashok et al.*, 2007; *Hendon et al.*, 2009; *Larkin and Harrison*, 2005b; *Lim et al.*, 2009; *Wang and Hendon*, 2007; *Weng et al.*, 2007, 2009], the Indian monsoon [*Kumar et al.*, 2006], and the frequency of tropical cyclones in the North Atlantic [*Kim et al.*, 2009]. These differences in teleconnection patterns between cold tongue and warm pool El Niño can introduce a large bias in paleo-ENSO reconstructions from extratropical locations, stressing the need for high-resolution records from all regions of the tropical Pacific. In order to capture the prehistoric occurrence of the two types of ENSO, these reconstructions should include records from the western tropical Pacific. This is because temperature anomalies in the eastern tropical Pacific are of opposite signs during CP and EP ENSO events.

2.2. The Oceanography of the Indonesian Seas

[8] The MD77 sediment core (Figure 1) was collected as part of the IMAGES program using the R.V. *Marion Dufresne*. The core location is at the northern entrance of the Makassar Strait (1.4°N, 119°E, and 968m depth) in the Sulawesi Sea. The Indonesian Sea, including the Sulawesi Sea is part of the Indo-Pacific Warm Pool, the largest reservoir of warm surface waters in the tropical Pacific. This is the source of moist static energy for the rising limb of the Hadley and Walker circulation cells [*Qu et al.*, 2005]. Therefore, changes in SSTs in the region can directly impact global atmospheric circulation. Surface ocean variability within the Makassar Strait is strongly influenced by the

seasonal monsoons and the position of the Inter-Tropical Convergence Zone (ITCZ), and to a lesser extent by ENSO [*Gordon*, 2005]. The Makassar Strait is part of the so-called Indonesian Seaway, which is the primary conduit for exchange of Pacific waters with the Indian Ocean and therefore, a critical part of the thermohaline circulation system [*Bray et al.*, 1996; *Gordon*, 1986]. The transport of upper ocean waters from the North Pacific through the Makassar Strait to the Indian Ocean, referred to as the Indonesian Throughflow (ITF), occurs primarily within the thermocline (100–200m, [*Sprintall*, 2009; *Susanto and Gordon*, 2005]). Approximately 80% of the ITF flows through the Makassar Strait [*Gordon*, 2005]. At the MD77 core location, the bulk of the ITF is composed of North Pacific subtropical water that flows southward from the Mindanao Current, east of the Philippines [*Sprintall*, 2009, Figure 1]. Thermocline temperature and salinity changes are primarily controlled by the seasonal reversal of winds that accompany the East Asian and Australian monsoons and also ENSO on an interannual timescale [*Gordon*, 2005].

[9] Seasonal changes in ITF properties and the net transport of water from the Pacific to the Indian Ocean are largely driven by the seasonal changes in monsoonal winds. The ITF transport through the thermocline intensifies during both monsoon seasons [*Gordon*, 2005; *Gordon et al.*, 2008]. During the Australian (northwestern) monsoon, wind-forcing results in a transport of the lower-salinity and more buoyant Java Seawater into the Makassar Strait, creating a surface "plug," which is accompanied by an increased transport within the thermocline [*Gordon*, 2005; *Gordon et al.*, 2003; *Susanto and Gordon*, 2005]. The southeastern monsoon winds constrain southward surface water flow out of the Makassar Strait, also enhancing thermocline transport from July to September [*Gordon*, 2005; *Gordon et al.*, 2003]. Transport of waters within the thermocline is highest and shallowest (lowest and deepest) during the southeastern (northwestern) monsoon [*Gordon et al.*, 2008].

[10] Since the ITF is primarily driven by the difference in sea level height between the western tropical Pacific and the Indian Ocean, the transport and water mass properties of the ITF also vary with ENSO. The weakening of the trade winds and the associated displacement of the western Pacific warm pool that occurs during an El Niño reduces the sea level gradient between the two ocean basins, reducing the ITF transport [*Bray et al.*, 1996; *England and Huang*, 2005; *Fieux et al.*, 1996; *Gordon*, 2005; *Gordon and Fine*, 1996; *Gordon and Susanto*, 1999; *Gordon et al.*, 1999; *Meyers*, 1996; *Sprintall*, 2009]. A 15-year database of XBT (Expendable Bathythermograph) data has shown that thermocline temperatures in the Makassar Strait are highly correlated (r = 0.77) with the SOI [*Ffield et al.*, 2000]. Unfortunately, there is no long, continuous in situ temperature and salinity data at the MD77 site. We therefore rely on reanalysis data to evaluate the impact of ENSO and the seasonal cycle on temperature and salinity at the surface and within the thermocline at the core location. We use the European Center for Medium-Range Weather Forecasts (ECMWF) ocean reanalysis system 3 covering the period 1959–2009 (thereafter, ORA-S3, [*Balmaseda et al.*, 2008]). Our motivation for using the ORA-S3 reanalysis compared to other reanalysis data sets stems from the fact that the artificial vertical velocity fields produced by most ocean models within a few degrees of the

equator [*Bell et al.*, 2004] are partially corrected for through the use of an online bias-correction scheme in the pressure field [*Balmaseda et al.*, 2007, 2008]. In the absence of this bias-correction algorithm, the artificial velocity field can produce inaccuracies in the temperature estimates [*Bell et al.*, 2004], making an evaluation of ENSO dynamics at the MD77 location impossible. We acknowledge that the reanalysis data may not be completely accurate (a fact further discussed in section 3) but it provides a basis for discussing the impact of ENSO at the MD77 site.

[11] Temperature and salinity anomalies were calculated for the ORA-S3 data set by removing the annual mean temperature (salinity) of the entire reanalysis period at each depth. Any long-term trends in the data were not removed beforehand in order to evaluate the relative strength of the interannual signal and background climate variability. Temperature anomalies associated with ENSO dynamics at the MD77 location are greater within the thermocline than in the mixed layer. The maximum anomalies occur at ~100m depth and average $\sim \pm 2°C$. In the upper thermocline, the temperature anomalies associated with ENSO are on the order of $\sim \pm 1°C$ (Figure 1b). On the other hand, salinity changes are largely independent of ENSO (Figure 1c). At the surface, the lack of an ENSO-salinity relationship is explained by the long-term decrease (~1psu) in salinity from 1959 to 1982 apparent in the ORA-S3 reanalysis data set, which masks the interannual variability. Changes in salinity in the sub-surface are small (<0.1psu) and are not systematically associated with ENSO, although there is a general tendency toward slightly lower (higher) salinities during La Niña (El Niño). However, the interannual anomalies in salinity are of the same magnitude as those associated with the seasonal cycle (Figure 1e). On the other hand, the seasonal changes in temperature, which can conceal the surface expression associated with ENSO, are reduced in the thermocline, which enhances the expression of ENSO (Figure 1d). At the core location the thermocline temperature (and, to a lesser extent, salinity) anomalies that accompany CP and EP types of ENSO are of the same magnitude and most importantly, of the same sign. This means that the MD77 record is particularly well-suited for documenting the evolution of both types of ENSO events during the past millennium.

3. Modeling $\delta^{18}O$ of Individual *Pulleniatina obliquiloculata* in the Western Tropical Pacific

[12] Since individual planktonic foraminifera have an average lifespan of 2–4 weeks [*Spero*, 1998], a suite of $\delta^{18}O$ measurements for individual foraminiferal tests (~50–100) provides a composite sample of thermocline hydrographic variability, including that associated with ENSO [*Koutavas et al.*, 2006; *Leduc et al.*, 2009]. *Pulleniatina obliquiloculata* is a warm-water planktonic foraminifer commonly found in upper thermocline waters in tropical to subtropical regions [*Cléroux et al.*, 2007; *Wejnert et al.*, 2010]. The calcification depth of *P. obliquiloculata* depends on its ontogenic life cycle with juveniles mainly confined to the mixed layer before migration at greater depth at the time of cortex formation [*Erez and Honjo*, 1981; *Hemleben et al.*, 1989; *Ravelo and Fairbanks*, 1992]. This was demonstrated in a plankton tow study from the central equatorial Pacific where the largest abundance of adult specimens of

P. obliquiloculata were found below 60m [*Watkins et al.*, 1996]. Adult specimens of *P. obliquiloculata* can be easily identified from juveniles by the distinctive smooth outer cortex that envelops the final whorl in the adult, and an arched aperture [*Watkins et al.*, 1996]. A sediment trap study from south of Java reports calcification depths for this species between 60 and 80m [*Mohtadi et al.*, 2009], which we use as a basis for further assessing the impact of ENSO and the seasonal cycle on the $\delta^{18}O$ distributions of individual specimens of *P. obliquiloculata*.

[13] The $\delta^{18}O_{calcite}$ of *P. obliquiloculata* will vary with both temperature and the isotopic composition of seawater ($\delta^{18}O_{sw}$), the latter reflecting local salinity (and on longer time scales, ice volume changes). Since the contribution of ice volume to the $\delta^{18}O_{sw}$ over the past millennium can be neglected, the $\delta^{18}O_{calcite}$ is interpreted here only in terms of local temperature and salinity. We calculated monthly mean equilibrium $\delta^{18}O_{calcite}$ values at different depths between 1959 and 2009 from monthly temperature and salinity data taken from the ORA-S3 reanalysis data set. Evaporation, precipitation, advection, mixing, and river runoff are the physical processes that govern changes in salinity (and $\delta^{18}O_{sw}$) at the study site [*Benway and Mix*, 2004]. There have been several empirical $\delta^{18}O_{sw}$-salinity relationships proposed for the surface waters of the tropical Pacific, including the western tropical Pacific. These relationships were derived from either in situ observations [*Fairbanks et al.*, 1997; *Morimoto et al.*, 2002] or from isotope-enabled climate models [*LeGrande and Schmidt*, 2006]. The slopes of these $\delta^{18}O_{sw}$-salinity relationships vary between 0.27‰/psu [*Fairbanks et al.*, 1997; *LeGrande and Schmidt*, 2006] and 0.42‰/psu [*Morimoto et al.*, 2002]. Differences in the slope of the $\delta^{18}O_{sw}$-SSS relationship may reflect a large range of evaporation/precipitation conditions across the tropical oceans. Furthermore, these relationships are derived for surface waters and therefore, may not apply to the western Pacific thermocline waters as shown in another study from the Panama Strait in the eastern equatorial Pacific [*Benway and Mix*, 2004]. At that location, the slope of surface waters $\delta^{18}O_{sw}$-salinity relationship is 0.25‰/psu [*Benway and Mix*, 2004], close to the values reported by *Fairbanks et al.* [1997] and *LeGrande and Schmidt* [2006], whereas the slope of thermocline waters (40–100m) $\delta^{18}O_{sw}$-salinity is 0.47‰/psu, closer to the value reported by *Morimoto et al.* [2002]. For the present study modeled salinity values have been converted to $\delta^{18}O_{sw}$ using a linear $\delta^{18}O_{sw}$-salinity relationship where $\delta^{18}O_{sw}$ (VSMOW) = $0.42 \times$ Salinity(psu) $- 14.3$, following *Morimoto et al.* [2002]. The equilibrium $\delta^{18}O_{calcite}$ was then calculated from the species-specific paleotemperature equation of *Russell and Spero* [2000]: $T(°C) = 16.5 - 4.8(\delta^{18}O_{calcite}(VPDB) - \delta^{18}O_{sw}(VPDB))$ and the VSMOW-VPDB conversion of $\delta^{18}O_{sw}(VPDB) = \delta^{18}O_{sw}(VSMOW) - 0.27‰$ [*Bemis et al.*, 1998].

[14] The total range of $\delta^{18}O_{calcite}$ values for the 55–85m depth range that are expressed in the ORA-S3 reanalysis data set is 1.73‰. This large range in $\delta^{18}O_{calcite}$ is indicative of the temperature and salinity variability that accompanies the seasonal cycle, ENSO, and the range of calcification depths for *P. obliquiloculata*. In the following sections we present results of an analysis that distinguishes how the different environmental parameters influence a distribution

a.

b.

c.
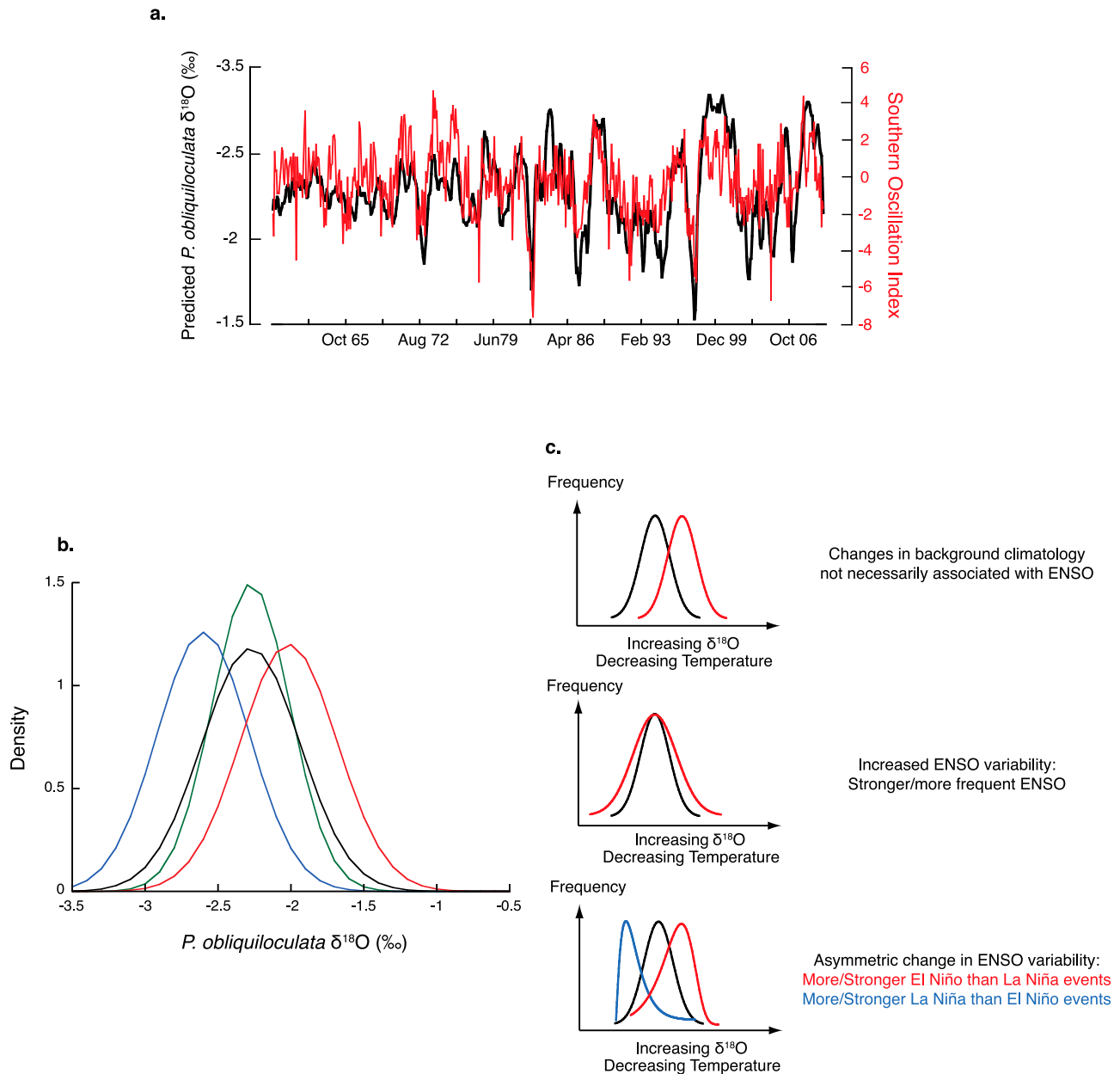
Figure 2. (a) Calculated monthly $\delta^{18}O_{calcite}$ for *P. obliquiloculata* (black curve) compared to the SOI (red curve). (b) Probability distribution function (PDF) of the calculated $\delta^{18}O$ values of *P. obliquiloculata* that would calcify during El Niño (red), La Niña (blue) and normal (green) years. The black curve represents the overall $\delta^{18}O$ distributions for the period 1959–2009. Each distribution represents the combined effect of the seasonal cycle, inter-ENSO and interannual variability and the range of calcification depths that apply to *P. obliquiloculata*. (c) Theoretical model for interpreting the statistics of the distributions in terms of ENSO variability (adapted from *Leduc et al.* [2009]).

of $\delta^{18}O$ values within a population of *P. obliquiloculata* and in doing so how the ENSO influence can be differentiated.

3.1. The Influence of ENSO on $\delta^{18}O$ Distributions

[15] The monthly calculated $\delta^{18}O_{calcite}$ values at the calcification depths of *P. obliquiloculata* exhibit a strong interannual variability that correlates significantly with the southern oscillation index (SOI, r = −0.54 at the 90% significant level, effective degrees of freedom corrected for persistence in the data set N_{eff} = 11, Figure 2a). The inter-

annual variability at the beginning of the ORA-S3 record is reduced compared to the end of the record, which may indicate a bias in the reanalysis as the number of available observations decreases. Indeed, when considering the post-1972 period, the correlation between the monthly calculated $\delta^{18}O_{calcite}$ and the SOI increases to r = −0.58 (90% significance level, N_{eff} = 7). This also implies that the temperature anomalies associated with ENSO may be slightly larger at this site than inferred from the reanalysis. In order to investigate how well the reanalysis captures ENSO vari-

ability, we compare the ORA-S3 data set to the NOAA consensus list of El Niño and La Niña years, which is based on the Oceanic Niño Index (ONI). According to the ONI index, an ENSO event is defined as 5 consecutive seasons (3-month running average) with an absolute temperature anomaly greater than 0.5°C in the Niño 3.4 region (5°N–5°S, 120°–170°W), based on the 1971–2000 climatology (http://ggweather.com/enso/oni.htm). When applying this criterion to the temperature data set extracted from the ORA-S3 reanalysis in the Niño 3.4 region, 15 out of the 16 El Niño events occurring over the reanalysis period can be accurately predicted. The reanalysis also produces a false positive, predicting an El Niño in 1992–1993. Further, we are able to accurately predict 13 of the 15 La Niña events occurring during the same period, with no false positive. We define an ENSO event at the MD77 site as 5 consecutive seasons (based on a 3-month running average of the predicted $\delta^{18}O_{calcite}$) with an absolute anomaly greater than one standard deviation (0.2‰) based on the 1971–2000 climatology. When taking into consideration the entire reanalysis period, this criterion predicts El Niño (La Niña) events with 56% (40%) accuracy when using the NOAA ONI index and 63% (46%) accuracy when using the same index derived from the ORA-S3 reanalysis. This criterion also produces three false positives, predicting an El Niño event in 1992–1993 and a La Niña in 1978–1979 and 2008–2009. When considering the period after 1972, this criterion becomes 75% (83%) accurate in predicting El Niño and 60% accurate in predicting La Niña.

[16] The modeled $\delta^{18}O$ distributions depicted in black on Figure 2b reflect the accumulated $\delta^{18}O$ values of planktonic foraminifera that calcify during El Niño, La Niña, and during normal years. A year is defined here as May to the following April to emphasize the seasonal phase locking of the ENSO cycle. The El Niño and La Niña years are identified using the criterion based on the anomalies in $\delta^{18}O_{calcite}$ defined previously. Each distribution incorporates the influence of the seasonal cycle, inter-annual and inter-ENSO variability, and the range of calcification depths associated with *P. obliquiloculata*. The effect of intra and interannual changes in the production of *P. obliquiloculata* on the overall $\delta^{18}O$ distribution (black curve on Figure 2b) is addressed in section 3.4. The warmer (cooler) conditions such as those that accompany La Niña (El Niño) lead to lower (higher) population mean $\delta^{18}O$ values as illustrated on Figure 2b. Although there is a significant amount of overlap, the means of the distributions are significantly different (90% confidence level on a Student's t-test, N_{eff} = 430).

[17] An increase in the strength (taken here as to represent the amplitude of the temperature anomalies) and/or frequency of ENSO (both El Niño and La Niña) events will accentuate the difference in the mean of El Niño and La Niña distributions, resulting in an increase in the spread of the overall distribution, as measured by the standard deviation [*Koutavas et al.*, 2006; *Leduc et al.*, 2009, Figure 2c]. The standard deviation of the distribution for normal years is 0.27‰ compared to 0.34‰ for the overall distribution. This change in spread between a full ENSO model and no ENSO is significant at the 90% confidence level using a Fischer *F* test. Doubling (tripling) the number of ENSO events result in an increase in the standard deviation of 0.03‰ (0.04‰)

compared to the original overall distribution, a change that is significant at the 90% confidence level using the *F* test.

[18] On the other hand, an asymmetric change in ENSO variability will induce an asymmetry in the $\delta^{18}O$ distributions such that stronger or more frequent El Niños (La Niñas) will result in a negative (positive) skewness [*Leduc et al.*, 2009, Figure 2c]. Doubling the number of El Niño (La Niña) compared to normal and La Niña (El Niño) years does not result in an asymmetric distribution. On the other hand, tripling and quadrupling the number of El Niño (La Niña) years result in a change in the Pearson's coefficient of skewness of −0.04‰ and −0.06‰ (0.05‰ and 0.10‰) respectively, which is significant at the 90% significant level. In order to test for the significance of the asymmetry of the modeled $\delta^{18}O$ distributions, we use a procedure introduced by *Lanzante* [1996], which is summarized here. The method consists of partitioning the original distribution into two subsamples; one representing the values greater than the median and the other representing the values on the other side of the median, which have been reflected across the median [*Lanzante*, 1996]. If the original distribution is symmetric, then the medians of the two partitions should be identical. Here, we use a robust rank-order test, based on the Wilcoxon-Mann-Whitney test, for assessing the equality of the medians.

[19] It is interesting, to note that the trend toward stronger El Niños in the late 20th century reported in some earlier studies [*An and Jin*, 2004; *Burgers and Stephenson*, 1999; *Hannachi et al.*, 2003; *Jin et al.*, 2003; *Lau and Weng*, 1999; *Monahan and Dai*, 2004; *Rayner et al.*, 2003; *Trenberth*, 1997] is not reflected in the skewness of the ORA-S3 data set. The Pearson's coefficient of skewness for the overall distribution is −0.04‰, which is not statistically significant at the 90% confidence level. This could be due to either the reanalysis model itself, as general circulation models do not generally simulate this bias [*Guilyardi et al.*, 2009] or, to a weaker El Niño signal in the region because of changes in ITF transport that accompanies ENSO.

3.2. The Influence of the Seasonal Cycle and Background Climate on $\delta^{18}O$ Distributions

[20] Changes in the spread and to some extent the skewness may also be influenced by changes in the magnitude of the seasonal cycle and/or the magnitude of the interannual variability that is not associated with ENSO. In other words, a change in the spread of the overall distribution could be induced by changes in the spread of the $\delta^{18}O$ distributions for planktonic foraminifera that calcify during La Niña, El Niño, and normal years rather than from a change in ENSO variability itself. Therefore, to estimate the potential influence of changes in seasonality on the $\delta^{18}O$ distributions, we remove the seasonal cycle from the ORA-S3 reanalysis. This yields a standard deviation of 0.34‰ for the overall distribution, which is indistinguishable from the original value. Therefore, changes in the seasonal cycle do not significantly impact the statistics of the $\delta^{18}O$ distributions. This experiment also suggests that most of the variability depicted in the distribution functions is due to the varying strength of ENSO itself rather than the seasonal cycle.

[21] A shift in the background climate could also affect the measured $\delta^{18}O$ distributions. A step change in background climate during the period represented in the sediment sample

results in bimodal distributions [*Leduc et al.*, 2009], which cannot be interpreted in terms of ENSO variability. A gradual change in temperature could mask some, if not all, of the interannual variability associated with ENSO. The temperature difference between El Niño and La Niña events at our study site is ~1.6°C. If an increase of this magnitude occurred during a sampled period, the years at the beginning (end) of the time interval would plot as El Niño (La Niña) years in Figure 2b, and the thermocline variability reflected in the spread of the $\delta^{18}O$ distributions would be mostly attributable to the background warming. However, considering the high sediment accumulation rate that characterizes the MD77 core location, such a temperature change would have to occur within a period of 10–30 years (although the effective time slice is probably larger due to bioturbation, as noted later), a very unlikely scenario since, for example, changes in thermocline temperatures over the last glacial/interglacial cycle were on the order of 1.9°C [*Xu et al.*, 2008] in the region as estimated from *P. obliquiloculata* Mg/Ca. However, smaller long-term temperature trends may mask or amplify some of the ENSO variability that we infer from the spread of the $\delta^{18}O$ distributions.

3.3. The Influence of Calcification Depths on $\delta^{18}O$ Distributions

[22] Changes in the range of calcification depth could have a profound effect on the interpretation of the spread of the $\delta^{18}O$ distributions as a measure of ENSO variability. If only a few individuals calcified deeper (or shallower) during a specific time interval, their $\delta^{18}O$ values may be significantly higher (or lower) than the majority of specimens within the analyzed population and therefore would plot as outliers on a histogram of $\delta^{18}O$ values. Furthermore, changes in the overall calcification depth (for instance from 55 to 85m to 75–105m) of a large portion of the individuals analyzed from a single sample horizon would produce a bimodal distribution, which is not interpretable in terms of ENSO variability.

[23] An increase in the overall range of calcification depths from 30m to 45m would increase the standard deviation of the calculated $\delta^{18}O_{calcite}$ distribution by 0.10‰, which is significant at the 90% confidence level using the *F* test. Similarly, if a distribution of individual *P. obliquiloculata* were skewed because the preferred calcification horizon of *P. obliquiloculata* shoaled (or became deeper), this would induce asymmetry to a $\delta^{18}O$ distribution that would be misinterpreted as a change in ENSO variability. Consequently, an additional measure of the depth of calcification is needed. The sharp gradient in $\delta^{18}O_{calcite}$ within the thermocline is echoed in the $\delta^{13}C$ of dissolved ΣCO_2 (Figure S1 in the auxiliary material).[1] A change in the spread and symmetry of the $\delta^{13}C$ can therefore be used in combination with the $\delta^{18}O$ distribution to decipher the ENSO influence from any change in habitat. Specifically, a simultaneous increase (decrease) in the standard deviation of the measured $\delta^{18}O$ and $\delta^{13}C$ values is most likely to indicate a change in the range of habitat depths while opposite changes or no change in the spread of a $\delta^{13}C$ distribution would be indicative of shifts in ENSO variability rather than shifting habitat.

----

[1]Auxiliary materials are available in the HTML. doi:10.1029/2011PA002139.

Similarly, a positive (negative) skewness in the $\delta^{18}O$ ($\delta^{13}C$) distribution can be induced by an asymmetric population distribution in the water column toward a shallower habitat. On the other hand, if the sign of the skewness of the $\delta^{18}O$ and $\delta^{13}C$ distributions co-varies, then a change in skewness of a $\delta^{18}O$ distribution can be interpreted in terms of ENSO. This model relies on the notion the $\delta^{13}C$ of *P. obliquiloculata* reflects that of dissolved CO_2 or that the degree of isotopic disequilibrium remains constant. A study by *Mulitza et al.* [1999] showed that *P. obliquiloculata* does not secrete its test in isotopic equilibrium with dissolved CO_2, but the deviation from isotopic equilibrium is a linear function of temperature. Therefore, although the mean of the $\delta^{13}C$ cannot be used to infer the actual calcification depth, the spread and skewness of the individual $\delta^{13}C$ measurements should still be representative of the range of calcification depth and habitat preference within the thermocline.

[24] We acknowledge that our approach has several caveats. First, changes in ITF transport related to ENSO [*Bray et al.*, 1996; *England and Huang*, 2005; *Fieux et al.*, 1996; *Gordon*, 2005; *Gordon and Fine*, 1996; *Gordon and Susanto*, 1999; *Gordon et al.*, 1999; *Meyers*, 1996; *Sprintall*, 2009] may affect the thermocline $\delta^{13}C$ gradient. However, since no time series of apparent oxygen utilization is available for this location, the effect of interannual variability on the thermocline $\delta^{13}C$ gradient cannot be quantified. Second, our method can contain false negatives since a large change in ENSO variability can be compensated by a reduced range of habitat depth, leaving the statistics of the $\delta^{18}O$ distributions unchanged, which we use as our main proxy for ENSO variability. Nevertheless, the statistics of the $\delta^{13}C$ distributions provide a basis for assessing how depth habitat influences our interpretation of past ENSO variability (see section 5).

3.4. The Influence of Productivity on $\delta^{18}O$ Distributions

[25] The thermocline temperature and salinity changes that accompany the annual monsoon cycle, and to a lesser extent ENSO variability, may influence and change the production and flux of planktonic foraminifera, including *P. obliquiloculata*. A change in the production or flux would affect the distribution of $\delta^{18}O$ values. During the southeastern monsoon (JAS), large areas off the southwest coast of Sumatra, the southwestern part of the Makassar Strait, the south coast of Java, the Banda Sea, the Arafura Sea, and the south coast of Bali experience upwelling [*Tomascik et al.*, 1997]. This seasonal upwelling is particularly evident in the chlorophyll distribution derived from satellite data [*Qu et al.*, 2005] and in the large increase in primary productivity [*Kinkade et al.*, 1997]. It is also evident in foraminiferal fluxes documented in a sediment trap study conducted south of Java [*Mohtadi et al.*, 2009]. At that site, nearly 45% of the yearly *P. obliquiloculata* production is associated with the strong upwelling during the southeastern monsoon (JAS) whereas the lowest production occurs during the northwestern monsoon [*Mohtadi et al.*, 2009]. However, at the MD77 site primary productivity increases from 0.53 ± 0.36 gCm^{-2}day^{-1} during the southeastern monsoon to 1.23 ± 0.22 gCm^{-2}day^{-1} during the northwestern monsoon when river runoff is highest [*Kinkade et al.*, 1997]. We therefore expect the yearly *P. obliquiloculata* production to be weighted toward the boreal winter season. On an interannual

Table 1. Changes in the Standard Deviation and the Pearson's Coefficient of Skewness of the Modeled $\delta^{18}O$ Distributions Associated With the Variability in the Production of *P. obliquiloculata*

	Unweighted	Scenario 1	Scenario 2	Scenario 3	Scenario 4
Standard Deviation	0.34	0.34[a] ± 0.00[b]	0.34[a] ± 0.00[b]	0.40[a] ± 0.00[b]	0.38[a] ± 0.00[b]
Pearson's Skewness	−0.04	−0.05[a] ± 0.03[b]	−0.02[a] ± 0.03[b]	−0.04[a] ± 0.04[b]	0.02[a] ± 0.04[b]

[a]Mean of the 1,000 Monte Carlo simulations.
[b]Plus or minus 2σ of the 1,000 Monte Carlo simulations.

timescale, the amplitude of JAS *P. obliquiloculata* production south of Java is also strongly influenced by ENSO, with JAS production 4 times greater than during a normal year [*Mohtadi et al.*, 2009]. At the MD77 site, the relationship between primary productivity and ENSO is largely unknown. However, if we consider that river runoff is the primary influence on primary productivity in the northern Makassar Strait, then primary productivity should be larger (lower) during La Niña (El Niño) when precipitation over the Indonesian archipelago is higher (lower).

[26] To evaluate how a change in the intra or interannual production and flux of this species influences the distribution of $\delta^{18}O$ values, the predicted monthly $\delta^{18}O$ values from the ORA-S3 reanalysis are weighted according to four different scenarios based on the changes in primary productivity and foraminiferal fluxes as inferred previously. In scenario 1 and 2 we assess how a change in the seasonal cycle influences the $\delta^{18}O$ distributions. In scenario 1 (Table 1), the yearly production of foraminifera is kept constant (~200 individuals). The calculated monthly $\delta^{18}O$ values for the entire ORA-S3 data set are then weighted so that JAS (DJF) represents between 25% and 60% (0–25%) of the yearly total *P. obliquiloculata* production. In scenario 2, we weight the monthly values so that DJF (JAS) represents between 25% and 60% (0–25%) of the yearly total *P. obliquiloculata* production, a scenario more consistent with the observed changes in primary productivity in the northern Makassar Strait [*Kinkade et al.*, 1997]. The next two sets of simulations are used to investigate how interannual variations in the production of *P. obliquiloculata* affect the $\delta^{18}O$ distributions. In scenario 3, the DJF production is increased 2 to 6 times compared to that of scenario 2, so that DJF would represent up to 90% of the total yearly production during a given ENSO year. In contrast, scenario 4 emphasizes the role of ENSO in controlling the interannual variations in the production of planktonic foraminifera. The DJF production is increased 2x to 6x compared to that of scenario 2, but only during La Niña years. One thousand Monte Carlo simulations are performed for each of these scenarios. The mean of the standard deviation and the Pearson's coefficient of skewness (±2σ) for the

1,000 simulations are compared to the statistics of the original (non-weighted) predicted $\delta^{18}O$ distribution (Table 1). Adding a seasonal productivity component does not affect the spread or the skewness of the $\delta^{18}O$ distributions in the first two scenarios presented. This indicates that intrannual changes in *P. obliquiloculata* production associated with the monsoon do not significantly affect the overall distribution of $\delta^{18}O$ values within a population, a result consistent with the small seasonal cycle associated with the monsoon (Figure 1). On the other hand, increasing productivity during the winter months of ENSO years result in an overall increase in the standard deviation of the $\delta^{18}O$ distributions. This result is not surprising since increasing the productivity during these years is essentially equivalent to increasing the number of ENSO years in the reanalysis data set, which is consistent with the ENSO model developed in section 3.1. An increase in the productivity during the La Niña years also results in a change in the statistics of the $\delta^{18}O$ distributions, with an increase in a spread of the $\delta^{18}O$ distributions as well as a shift toward a positive skewness, a result also consistent with the ENSO model developed in section 3.1. Therefore, if our inference about productivity is correct, La Niña events should be more readily recorded in the thermocline at the MD77 site, slightly biasing an ENSO reconstruction toward La Niña conditions.

4. Analytical Methods

4.1. Age Model for Marine Sediment Core MD98-2177

[27] An age model for core MD77 was constructed using a quadratic fit through 5 calibrated AMS dates (Table 2 and Figure 3). All ages were calibrated using the CALIB 6.00 software and the Marine09 calibration [*Stuiver and Reimer*, 1993] with a standard reservoir age correction (ΔR) of 74 ± 70 years estimated for South Borneo [*Southon et al.*, 2002]. The radiocarbon content of the sample taken at 12 cm indicates a modern age at this horizon; an age reversal supported by the presence of some excess Pb-210 (Table 3). On the other hand, both the ^{14}C and excess ^{210}Pb of uppermost sample suggest that the top of the core is older and does

Table 2. AMS Results for Core MD98-2177

Depth	AMS Laboratory[a]	CAMS Number	^{14}C Age	Standard Deviation	Calibrated Age (years A.D.)	Age Uncertainty (years A.D.)
0cm	LLNL	95299	580	±45	1852	±51
12cm	UCI	OS-38302	395	±90	>modern	N/A
50cm	LLNL	100234	1110	±60	1350	±69.5
94cm	LLNL	100235	1745	±45	730	±82.5
109cm	UCI	OS-38335	1870	±110	584	±135.5
130cm	LLNL	100236	2260	±45	168	±100.5

[a]UCI, University of California, Irvine; LLNL, Lawrence Livermore National Laboratory.
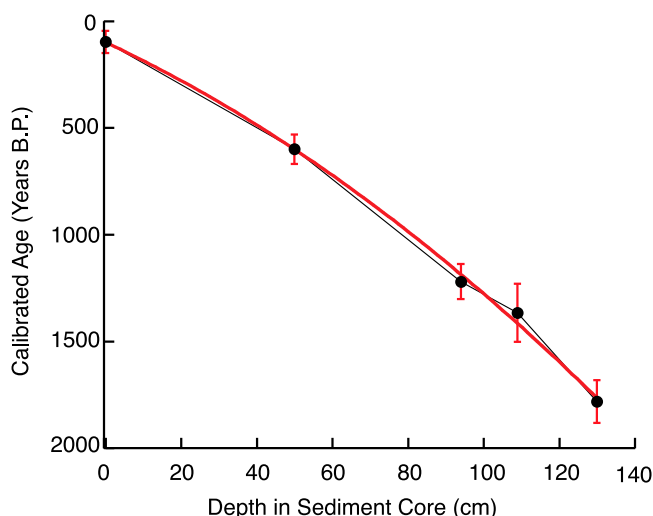
Figure 3. Age model for core MD98-2177 based on 5 AMS dates. The vertical error bars indicate the $\pm 1\sigma$ dating uncertainty, which comprises errors in the radiocarbon measurements as well as the errors associated with the calibration and the reservoir age. The red line shows the second-order polynomial fit used to construct the age model for core MD98-2177. The radiocarbon content of the sample taken at 12 cm indicates modern contamination and is not included to construct the age model.

not contain 20th century material. The reversal is assumed to be a result of bioturbation with the age reversal due to the localized presence of a burrow that contains some modern material. This indicates that the nominal dating uncertainty for each horizon in the MD77 core can be as large as 200 years, although the absence of further age reversals downcore suggests that this represents the upper limit of the dating uncertainty (Table 3). Furthermore, this uncertainty is not large enough to prevent a meaningful comparison between the MCA and the LIA, although it prevents comparisons between adjacent intervals.

[28] For the present study 1-cm to 2-cm intervals were sampled at 16 horizons in the MD77 sediment core. These intervals correspond to the MCA and LIA sections of the core (Table 4). Each 1-cm (2-cm) sediment interval represents ~10–30 years of accumulated sediment and foraminiferal tests, although the effective time slice for each sample may be larger. Based on modern excess ^{210}Pb measured in a sediment core from the Southern Makassar Strait [*Oppo et al.*, 2009], 2–5% of modern material might be present at ~12 cm. Using the upper estimate (5% of modern material mixed with material that is about 200 years older), we determine that the effective time slice for each horizon is 30–50 years. Furthermore, the core was sampled every ~5 cm; if we have underestimated the degree of bioturbation inferred from the radiocarbon and excess Pb-210 analysis, adjacent horizons in the sediment core may overlap in time.

4.2. Stable Isotope Methodology

[29] The bulk sediment samples from the MD77 core were disaggregated in a sodium hexametaphosphate solution and wet-sieved through a 63 μm mesh to remove the clay fraction. This >63 μm fraction was then dry-sieved at >250 μm.

The individual adult *P. obliquiloculata* were picked from this fraction under a binocular microscope. Adult specimens were differentiated from juveniles by the presence of a thick, smooth cortex layer. The foraminifera were then rinsed three times with deionized water (DIW), followed by a methanol rinse. The low viscosity of this reagent helps dislodge clays and other impurities from the carbonate tests [*Barker et al.*, 2003]. These steps are followed by a rinse with an alkali buffered 1% H_2O_2 solution designed to remove organic material, a weak acid leach to remove coarse-grain silicates contaminants [*Barker et al.*, 2003] and a final DIW/methanol rinse. The samples were sonified after each rinse to help dislodge any contaminants. The calcite preservation in MD77 sediment samples is excellent because the core was taken above the present-day lysocline and because it is characterized by very high sediment accumulation rates.

[30] Approximately 70 adult individual *P. obliquiloculata* were picked for each sample (time horizon), inspected for cleanliness under a microscope, weighed individually and then loaded into individual vials for stable isotope analysis. The median weights of the *P. obliquiloculata* used in this study vary between 18 and 25μg with a interquartile range between 8 and 13μg; suggesting that the individuals used for all climatic periods in this study were of similar size (Table 4). The δ^{13}C and δ^{18}O values were measured using a Multiprep Dual Inlet system attached to an Isoprime stable isotope ratio mass spectrometer. Each sequential run of the Multiprep included 30–50 individual foraminiferal samples together with 10–15 calcite standards of similar weight (USC Ultissima marble) used to monitor analytical precision. The long-term precision of the Ultissima standard δ^{13}C and δ^{18}O values measured during this study was 0.07‰ and 0.09‰ respectively. Individual foraminiferal tests from each discrete sample were run out-of-sequence in order to minimize the effect of analytical uncertainty on the difference in spread among the sampled intervals. There was no observed test weight to δ^{18}O or δ^{13}C relationship, suggesting that size was not a factor for depth habitat. A summary of the sedimentary and statistical results is presented in Table 4. The measured δ^{13}C, δ^{18}O and weights of the individual *P. obliquiloculata* are presented in Table S1 in the auxiliary material.

5. Results and Discussion: ENSO Changes Over the Past Millennium

5.1. ENSO Versus Calcification Depth

[31] Histograms of the δ^{18}O measurements performed on single specimen of *P. obliquiloculata* (Figure 4) indicate that in certain core intervals (especially during the MCA),

Table 3. The ^{210}Pb and ^{214}Pb Measurements for MD98-2177

| Depth	Layer Thickness	^{214}Pb ($\pm 1\sigma$) Bq/kg	^{210}Pb ($\pm 1\sigma$) Bq/kg	Excess ^{210}Pb ($\pm 1\sigma$) Bq/kg
2.5cm	0.8cm	68 ± 11	0 ± 115	–
3.3cm	0.4cm	84 ± 12	0 ± 150	–
3.7cm	0.4cm	69 ± 12	0 ± 172	–
11.5cm[a]	1cm	24 ± 4	53 ± 43	29 ± 43
11.5cm[a]	1cm	29 ± 6	82 ± 68	53 ± 68
12.5cm[a]	1cm	33 ± 3	84 ± 28	51 ± 28
12.5cm[a]	1cm	28 ± 4	61 ± 41	33 ± 41

[a]Duplicate samples.

Table 4. Sedimentary and Statistical Results for Each Time Slice

Age	1843–1851	1800–1817	1737–1755	1681–1700	1622–1642	1496–1518	1452–1464	1407–1419	1337–1349	1290–1302	1240–1265	1139–1165	1060–1087	895–923	793–823	704–734
Age Uncertainty (±1σ)	10	42	97	85	72	58	58	63	69	62	58	54	54	65	76	76
Sample width (cm)	1	2	2	2	2	2	1	1	1	1	2	2	2	2	2	2
Depth in core (cm)	0–1	4–6	11–13	17–19	23–25	35–37	40–41	44–45	50–51	54–55	58–60	65–67	71–73	83–85	90–92	96–98
Number of individuals analyzed	67	77	76	81	65	76	72	72	69	60	79	88	67	73	71	72
Median/mean weight of individuals analyzed (μg)	20/21	21/21	19/19	22/22	21/22	25/26	18/21	23/25	24/25	23/27	21/23	23/25	23/24	22/24	23/25	23/26
Interquartile range of weights of individuals analyzed (μg)	11	7	7	8	11	8	11	12	8	10	10	11	10	9	10	13
$\delta^{18}O$ Biweight Mean	-2.23	-2.26	-2.15	-2.15	-2.20	-2.12	-2.04	-2.00	-2.10	-2.07	-1.97	-1.98	-2.03	-2.05	-2.08	-2.17
$\delta^{18}O$ interquartile range (‰)	0.35	0.39	0.51	0.41	0.53	0.47	0.44	0.51	0.41	0.53	0.47	0.39	0.45	0.49	0.56	0.43
$\delta^{18}O$ BSD (‰)	0.28	0.34	0.39	0.34	0.38	0.32	0.35	0.40	0.36	0.41	0.38	0.34	0.34	0.39	0.38	0.30
$\delta^{18}O$ YKS	0.02	0.02	-0.10	-0.17	0.06	0.03	-0.08	0.16	0.02	0.10	0.49	0.03	0.35	-0.04	0.25	0.13
$\delta^{18}O$ $\sigma_{standard}$ (‰)	0.09	0.07	0.11	0.10	0.09	0.10	0.11	0.11	0.11	0.11	0.09	0.09	0.10	0.10	0.10	0.10
$\delta^{13}C$ Biweight Mean	0.75	0.77	0.85	0.84	0.89	0.86	0.78	0.77	0.78	0.74	0.84	0.82	0.81	0.80	0.77	0.70
$\delta^{13}C$ interquartile range	0.35	0.25	0.23	0.21	0.21	0.21	0.22	0.24	0.21	0.23	0.20	0.27	0.25	0.23	0.29	0.26
$\delta^{13}C$ BSD (‰)	0.24	0.18	0.18	0.17	0.15	0.18	0.18	0.19	0.15	0.19	0.15	0.24	0.18	0.16	0.19	0.19
$\delta^{13}C$ YKS	-0.15	-0.07	-0.21	-0.13	0.08	0.18	0.05	-0.18	0.00	0.28	0.07	0.04	0.01	-0.02	-0.22	0.19
$\delta^{13}C$ $\sigma_{standard}$ (‰)	0.05	0.08	0.07	0.09	0.08	0.09	0.05	0.05	0.05	0.06	0.06	0.09	0.08	0.06	0.06	0.05

the distribution of individual $\delta^{18}O$ values is not Gaussian. Therefore we apply robust statistics (i.e., insensitive to distributional assumptions) to quantify the moments of the $\delta^{18}O$ distributions. Furthermore, we need resistant statistics due to (1) the relatively small sample size and (2) the presence of outliers in the distributions. These outliers probably represent individuals of *P. obliquiloculata* that calcified deeper/shallower than the prescribed habitat depth of 55–85m inferred from the sediment trap conducted south of Java [*Mohtadi et al.*, 2009]. Specifically, we use the biweight standard deviation (hereafter, BSD [*Hoaglin et al.*, 1983; *Lanzante*, 1996]) and the Yule-Kendall skewness (YKS, also known as the Bowley or quartile coefficient of skewness [*Bowley*, 1920]) as measures of spread and of symmetry, respectively. The BSD is estimated through a two-step procedure. First, the median and the median absolute deviation are calculated for each distribution; these estimates are used to discard outliers [*Lanzante*, 1996]. The median absolute deviation is the median of the absolute deviations of the $\delta^{18}O$ values from the median of the distribution. Then a weighting scheme is applied such that values that are further away from the median are given less weight. In a Gaussian case, if a value falls more than 5 standard deviations away from the median, it is given a weight of zero [*Lanzante*, 1996]. Using resistant statistics reduces sensitivity to individuals that may have calcified deeper/shallower within the thermocline and allows evaluation of changes in the spread and symmetry associated with the bulk of the $\delta^{18}O$ distributions, reducing the sensitivity to individuals that may have calcified deeper/shallower within the thermocline.

[32] The BSD and YKS values for the $\delta^{13}C$ and $\delta^{18}O$ distributions for the sampled intervals are presented in Table 4. The BSD for the $\delta^{18}O$ distributions varies between 0.28‰ and 0.41‰, with an average of 0.36‰ similar to the 20th century average inferred from the ORA-S3 reanalysis data set for the calcification depths ascribed to *P. obliquiloculata*. Furthermore, the BSD of the $\delta^{18}O$ distributions has remained remarkably constant through time as shown by the lack of significant changes as measured by the Brown-Forsythe test for the analysis of variance [*Brown and Forsythe*, 1974]; this is a nonparametric test based on the absolute deviation from the median (Table 5). Similarly, there is almost no significant change in the BSD of the $\delta^{13}C$ distributions over the study period (Table 6), which suggests that the range of calcification depth for *P. obliquiloculata* has remained fairly constant over the past millennium. Other lines of evidence for a constant habitat range comes from a direct comparison between the location of the $\delta^{18}O$ distributions (quantified here using the biweight mean, a robust and resistant measure of location [*Lanzante*, 1996]) and that of the $\delta^{13}C$ distributions as well as the spread of the $\delta^{18}O$ distributions. A shift in the calcification depth of *P. obliquiloculata* should be reflected by a negative relationship between the biweight mean of the $\delta^{18}O$ and the $\delta^{13}C$ distributions. For instance, if *P. obliquiloculata* calcified deeper, the biweight mean of the $\delta^{18}O$ distribution should become more positive while the biweight mean of the $\delta^{13}C$ distributions should decrease (Figure S1). Such a relationship is not evident in our data set (Table 4, slope = 0.05, R^2 = 0.01, not significant at the 90% confidence level, N_{eff} = 16). Furthermore, assuming that the vertical distribution of *P. obliquiloculata* within the thermocline is Gaussian, an increase in the calcification range
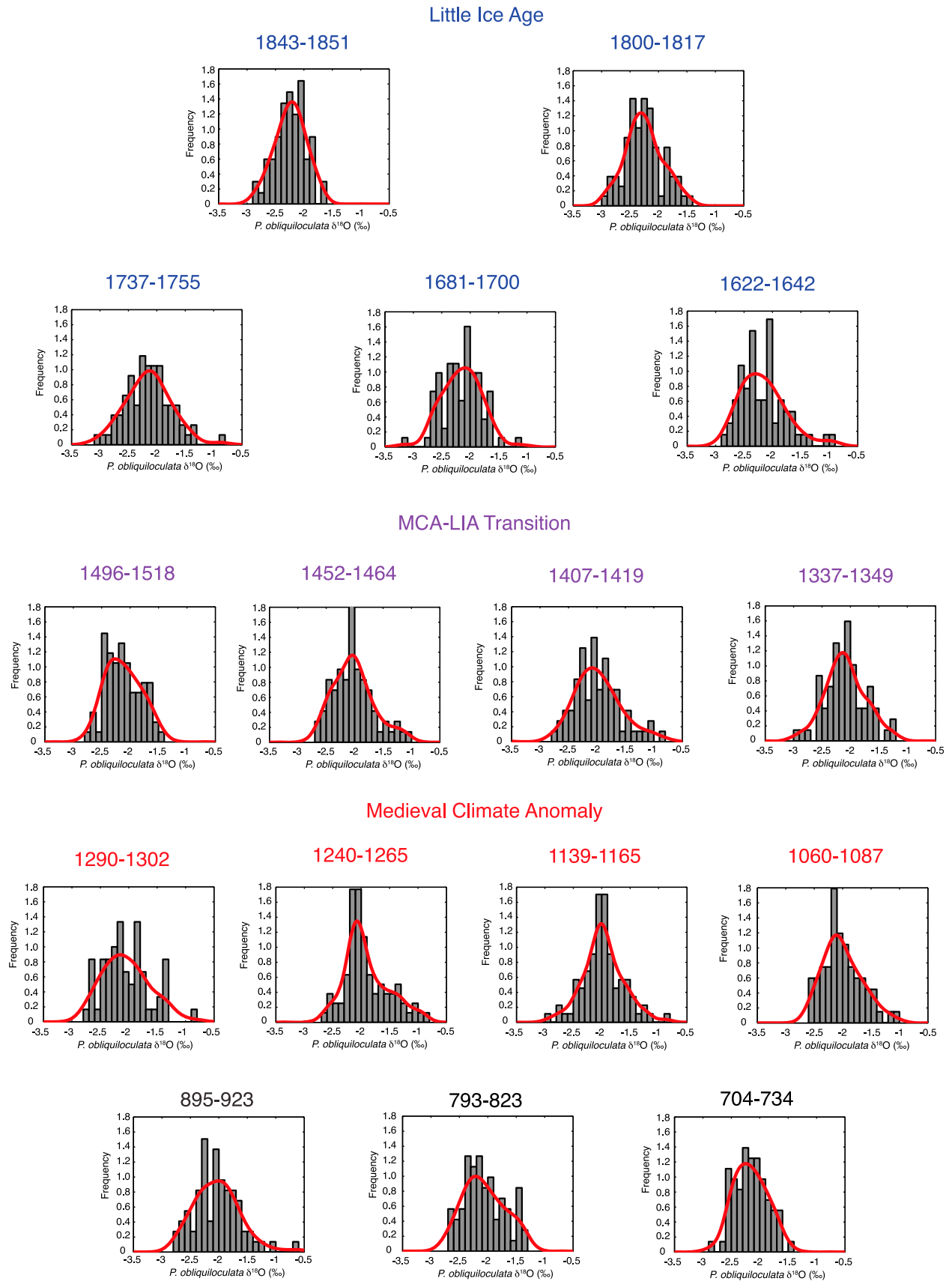
Figure 4. Histograms representing the frequency of individual *P. obliquiloculata* $\delta^{18}O$ values (binned into 0.1‰ intervals) with their respective Kernel density function (red curves) for each time slice.

Table 5. Test Matrix From the Brown-Forsythe Test for the Analysis of Variance Giving the Probability for Two Time Slices to Have a Different $\delta^{18}O$ Biweight Standard Deviation[a]

Age	1843–1851	1800–1817	1737–1755	1681–1700	1622–1642	1496–1518	1452–1464	1407–1419	1337–1349	1290–1302	1240–1265	1139–1165	1060–1087	895–923	793–823
1800–1817	X														
1737–1755	≥99	X													
1681–1700	≥90	X	X												
1622–1642	≥99	X	X	X											
1496–1518	X	X	≥90	X	≥90										
1452–1464	X	X	X	X	X	X									
1407–1419	≥99	≥90	X	X	X	≥90	X								
1337–1349	≥90	X	X	X	X	X	X	X							
1290–1302	≥99	≥90	X	X	X	≥95	X	X	X						
1240–1265	≥95	X	X	X	X	X	X	X	X	X					
1139–1165	X	X	X	X	X	X	X	X	X	X	X				
1060–1087	X	X	X	X	X	≥90	X	X	X	X	X	X			
895–923	≥99	X	X	X	X	X	X	X	X	X	X	X	X		
793–823	≥95	X	X	X	X	X	X	X	X	X	X	X	X	X	
704–734	X	X	≥95	X	≥95	X	X	≥95	X	≥95	X	X	X	≥95	≥90

[a]Probability in percent. X indicates that the biweight standard deviations of the two intervals are not statistically different (below the 90% confidence level).

Table 6. Test Matrix From the Brown-Forsythe Test for the Analysis of Variance Giving the Probability for Two Time Slices to Have a Different $\delta^{13}C$ Biweight Standard Deviation[a]

Age	1843–1851	1800–1817	1737–1755	1681–1700	1622–1642	1496–1518	1452–1464	1407–1419	1337–1349	1290–1302	1240–1265	1139–1165	1060–1087	895–923	793–823
1800–1817	≥95														
1737–1755	≥95	X													
1681–1700	≥99	X	X												
1622–1642	≥90	X	X	X											
1496–1518	≥90	X	X	X	X										
1452–1464	≥95	X	X	X	X	X									
1407–1419	X	X	X	X	X	X	X								
1337–1349	≥95	X	X	X	X	X	X	X							
1290–1302	≥95	X	X	X	X	X	X	X	X						
1240–1265	≥99	X	X	X	X	X	≥90	X	≥90	≥95					
1139–1165	X	≥95	≥95	≥99	X	X	X	X	X	≥95	≥99				
1060–1087	≥95	X	X	X	X	X	X	X	X	X	X	X			
895–923	≥99	X	X	X	X	X	X	X	X	X	X	≥99	X		
793–823	≥90	X	X	X	X	X	X	X	X	X	X	X	X	≥90	
704–734	≥95	X	X	X	X	X	X	X	X	X	X	≥90	X	X	X

[a]Probability is in percent. X indicates that the biweight standard deviations of the two intervals are not statistically different (below the 90% confidence level).

Table 7. Test Matrix Giving the Probability That the Distribution Is Asymmetric[a]

Age	$\delta^{18}O$ (%)	$\delta^{13}C$ (%)
1843–1851	X	X
1800–1817	X	X
1737–1755	X	≥90
1681–1700	≥95	X
1622–1642	X	X
1496–1518	X	X
1452–1464	X	X
1407–1419	X	≥95
1337–1349	X	X
1290–1302	≥90	X
1240–1265	≥99	X
1139–1165	X	X
1060–1087	≥99	X
895–923	X	X
793–823	≥99	≥99
704–734	X	X

[a]X represents symmetric distributions.

and depth would result in a more positive $\delta^{18}O$ biweight mean, representing a shift in the main body of the distribution as well as an increase in the BSD of the $\delta^{18}O$ distributions. However, such a relationship is not necessary to explain changes in the strength/frequency of ENSO since El Niño and La Niña events represent the tail of the distribution (Figure 2), and changes in the spread can then only be explained by an increase in the difference in the mean of El Niño and La Niña distributions, which would not affect the mean of the overall distribution. There is no apparent relationship between changes in the spread and the mean of the $\delta^{18}O$ distributions in our data set (Table 4, slope = 0.18, R^2 = 0.20, not significant at the 90% confidence level, N_{eff} = 16). Taken together, these three lines of evidence suggest that changes in the range of calcification depths may have played a minimal role in shaping the $\delta^{18}O$ record; therefore we interpret the spread and symmetry of the $\delta^{18}O$ distributions mostly in terms of ENSO.

5.2. Inferring ENSO Variability Over the Past Millennium

[33] Because the paired radiocarbon and excess Pb-210 measurements used to construct the age model for MD77 suggest that this core is bioturbated over a length of at least ~10 cm, adjacent distributions of $\delta^{18}O$ of individual specimens of *P. obliquiloculata* may represent the same time period. This implies that changes in the spread between two adjacent distributions may be representative of the reproducibility associated with the technique and the degree of mixing by bioturbation rather than changes in ENSO variability. However, bioturbation should not affect the reconstruction over centennial timescales. Furthermore, the time window inferred from our age model for each distribution is ~10–30 years, although the effective time slice is probably larger due to bioturbation (we estimate 30–50 years). This time windows may not be long enough to truly assess changes in ENSO variability. To take into account the effect of bioturbation and increase the effective time window in order to capture changes in ENSO variability over centennial timescales, we remove the mean of each distribution and group the $\delta^{18}O$ values into 4 time periods corresponding to the LIA (1500–1850A.D.), the MCA (800–1300A.D.) the
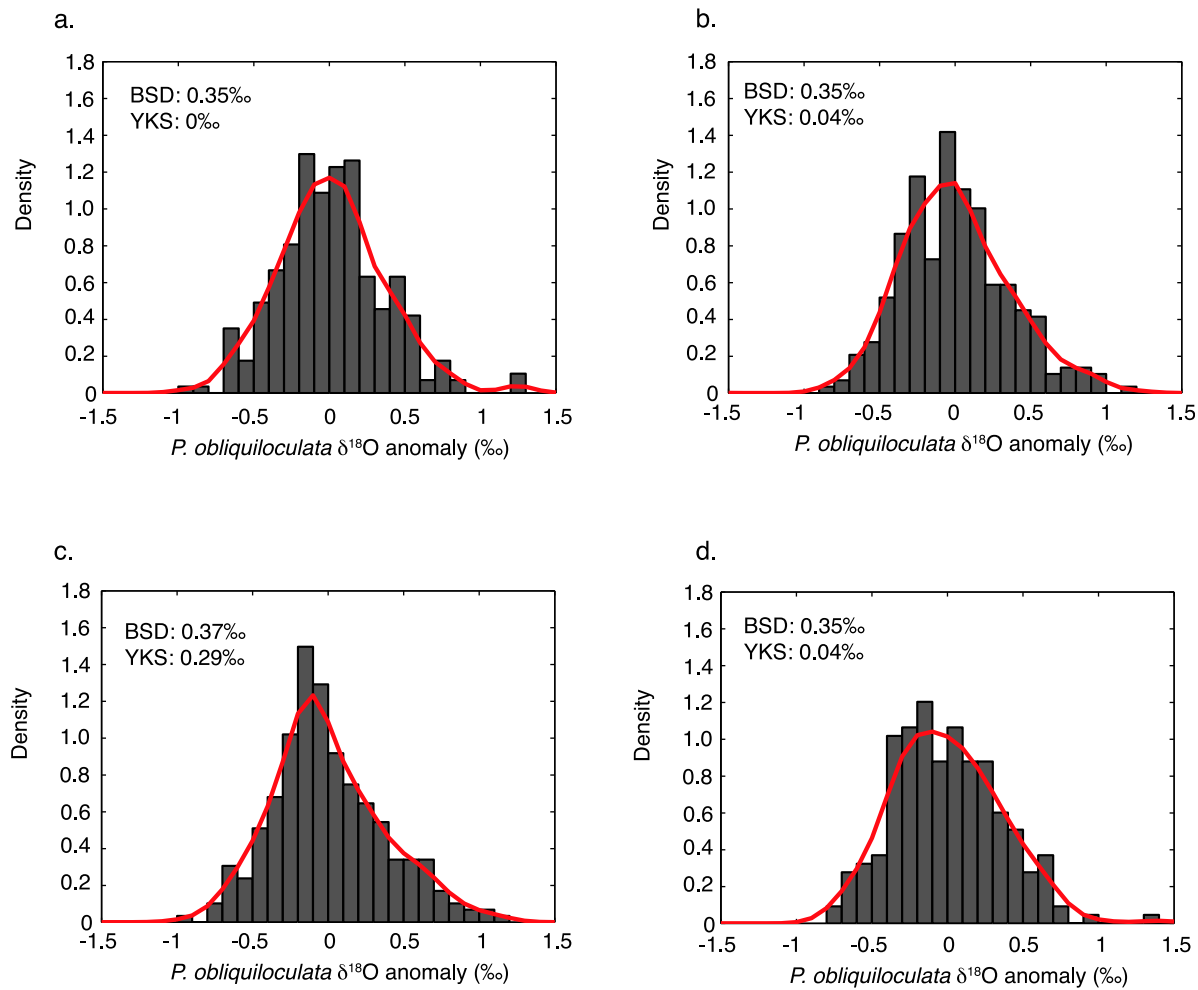
transition from the MCA to the LIA (1300–1400A.D.) and the Dark Ages Cold Period (450–750A.D.). Histograms of the $\delta^{18}O$ measurements performed on individual specimens of *P. obliquiloculata* for each of the 4 time periods are presented in Figure 5. The BSD value for each of these 4 periods is 0.35‰, 0.37‰, 0.35‰, and 0.35‰ respectively. The increase in the BSD value during the MCA is not significant at the 90% confidence level using the Brown-Forsythe tests for the analysis of variance. Indeed, one of the most notable features of our ENSO record from the western tropical Pacific is that there is no systematic difference in the strength/frequency of ENSO associated with the period broadly defined as the MCA and the LIA (Figure 6b).

[34] To compare our MD77 record to an ENSO reconstruction derived from a coral $\delta^{18}O$ record from Palmyra Island in the central equatorial Pacific [*Cobb et al.*, 2003], we apply a 2–7 year bandpass filter to the monthly resolved coral $\delta^{18}O$ record in order to isolate the variability associated with ENSO and then bin the $\delta^{18}O$ values into 20 to 50-year intervals. We then calculate the standard deviation for each bin (Table S2 and Figure 6c). The standard deviation for binned coral $\delta^{18}O$ values varies between 0.07‰ and 0.13‰, after exclusion of the 0.04‰ value that corresponds to a window of only 14 years. Albeit small, these differences are significant at the 90% confidence level (Table S3) and suggest that the LIA (standard deviation = 0.11‰) was characterized by periods of greater ENSO variability than the MCA (standard deviation = 0.08‰) or the 20th century (standard deviation = 0.10‰); a conclusion consistent with that of *Cobb et al.* [2003]. However, a closer examination of the record suggests that changes in ENSO variability within the MCA and the LIA have the same (or greater) magnitude than differences between the MCA and LIA. The standard deviation for the binned coral $\delta^{18}O$ values corresponding to the period ~900–1450 A.D. varies between 0.07‰ and 0.1‰; changes that are significant at the 90% confidence level using a *F* test (Table S3). Similarly, the standard deviation for the binned coral $\delta^{18}O$ values corresponding to LIA varies between 0.10‰ and 0.13‰. This 0.03% range within the MCA and LIA intervals is significant at the 90% confidence level (Table S3) and of similar magnitude as between the MCA and LIA intervals. A similar comparison for the MD77 record is more difficult because of bioturbation, especially for the intervals corresponding to the LIA. However, the BSD for the A.D. 1496–1518 intervals is significantly lower (90% confidence level, Table 5) than that for the A.D. 1290–1302 and A.D. 895–925 intervals. These intervals are located 18.5cm and 48cm apart, respectively, limiting the effect of biotubation on the statistics of the distribution. This analysis on our MD77 record suggests that changes in the strength/frequency of both El Niño and La Niña events are larger on decadal timescale than on centennial to millennial timescales.

5.3. El Niño Versus La Niña History

[35] In our western Pacific record, the period that corresponds to the MCA and the transition into the LIA is characterized by stronger/more frequent La Niñas than El Niños (Table 4 and Figure 7b) as evidenced by the presence of several significantly (Table 7) positively skewed $\delta^{18}O$ distributions during this time interval. When taken together in order to reduce the effect of bioturbation on the MD77

Figure 5. Histograms representing the frequency of individual *P. obliquiloculata* δ^{18}O values (binned into 0.1‰ intervals) with their respective Kernel density function (red curves) for the (a) LIA, (b) the transition from the LIA to the MCA, (c) the MCA and (d) the Dark Ages Cold Period. The spread of the δ^{18}O distributions, as measured by the BSD, is similar among these distributions. This suggests that ENSO strength/frequency has remained remarkably constant on centennial timescales over the past millennium. The MCA was also characterized by a positively skewed distribution, suggesting an increase in the relative strength/frequency of La Niña compared to El Niño.

record, the YKS value for the distributions corresponding to the MCA is 0.29‰, which is significant at the 90% significance level. This high YKS value is partly attributable to the assumed increase in *P. obliquiloculata* productivity during La Niña events (section 3.4), which reinforces the original positive skewness attributed to increased strength/frequency of La Niña compared to El Niño. This result is consistent with negative values for the Pearson's coefficient of skewness for the Palmyra coral δ^{18}O distributions (Tables S2 and S4 and Figure 7c) that indicate there was a departure toward stronger La Niña compared to El Niño between A.D. 1300 and A.D. 1450, which corresponds within age uncertainty to the positively skewed intervals between A.D.1240–1265 and A.D. 1290–1302 in the MD77 record.

[36] The MCA was a period characterized by recurrent widespread droughts over western North America as reconstructed from a network of drought-sensitive trees. These so-called medieval megadroughts occurred at A.D. 1021–1051, A.D. 1240–1265, and A.D. 1413–1460 [*Cook et al.*, 2004, Figure 7d; *Cook et al.*, 2007]. Modeling studies [*Burgman et al.*, 2010; *Herweijer et al.*, 2007; *Seager et al.*, 2008] link these megadroughts to La Niña-like conditions in the tropical Pacific. Such conditions are evident in the MD77 YKS record as well as in the relatively cooler and more saline (lower precipitation) conditions documented in δ^{18}O values of the Palmyra corals between A.D. 950 and A.D 1250 [*Cobb et al.*, 2003] as well as cooler conditions inferred from a diatom record from El Junco Lake, Galapagos [*Conroy et al.*, 2009]. However, this is in sharp contrast with studies by *Conroy et al.* [2008] and *Moy et al.* [2002], who inferred greater precipitation over the Galapagos and Southern Ecuador during the MCA, which the authors attributed to increased frequency of El Niño during that period. This discrepancy was pointed out by *Conroy et al.* [2010], who argued that these disparities are related to different factors
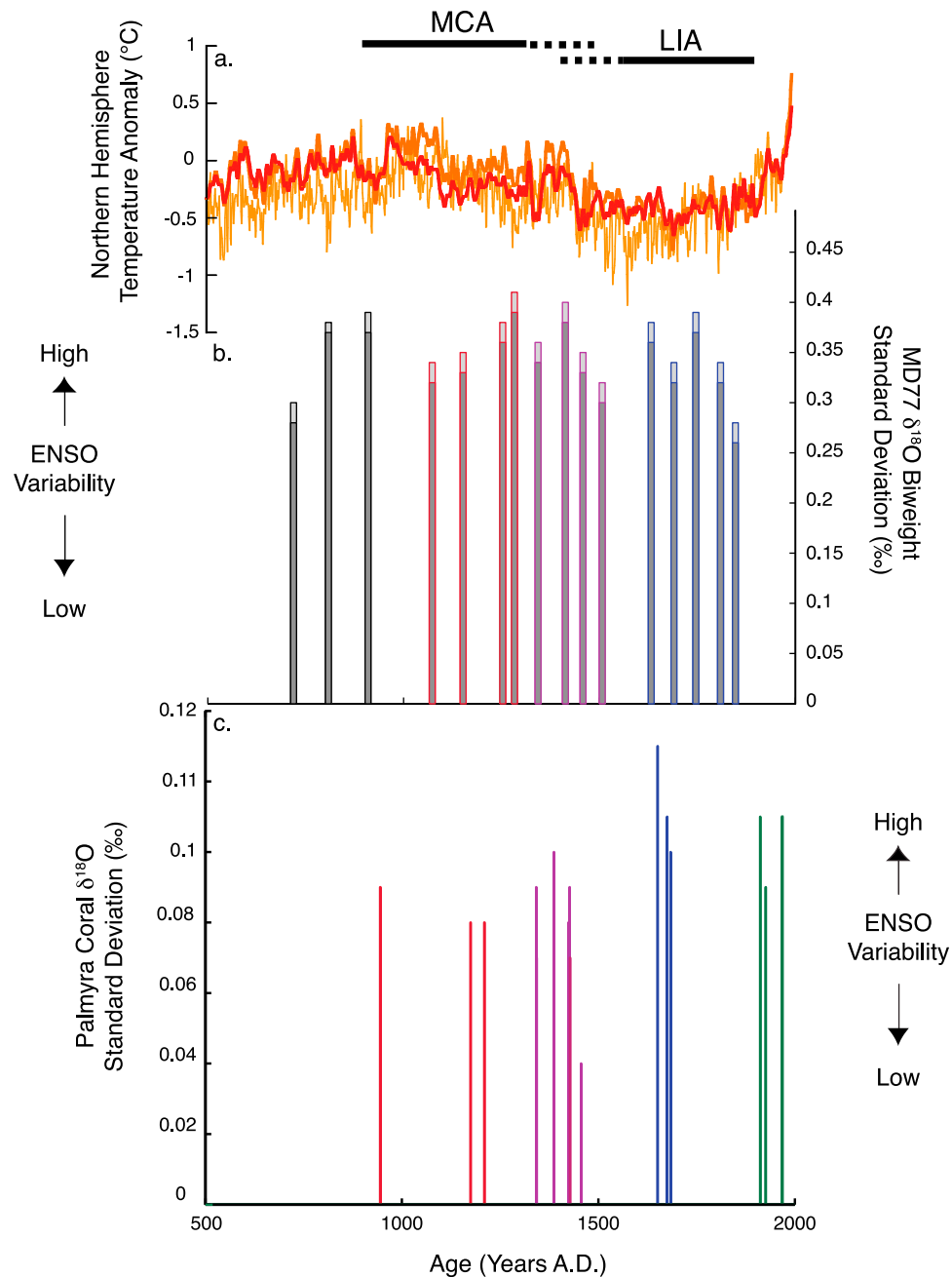
Figure 6. Changes in ENSO variability over the past millennium. (a) Northern Hemisphere temperature anomaly reconstructions from *Moberg et al.* [2005] (orange), and *Mann et al.* [2008] (land EIV temperature composite, dark orange, land + ocean EIV composite, red). (b) Biweight standard deviation values for each time slice sampled from MD98-2177. The light gray bars represent the BSD values for the entire data set. The dark gray bars represent the BSD values for the trimmed data set in which the highest and lowest $\delta^{18}O$ values were removed from the original data set. The statistics of the trimmed data set are not significantly different from that of the full distribution, which is consistent with the use of resistant statistics to quantify the moments of the distribution. Changes in ENSO variability, as measured by the BSD, are small and not significant on centennial time scale. (c) Standard deviation values for each time slice sampled from the Palmyra Island coral $\delta^{18}O$ record [*Cobb et al.*, 2003]. The blue, purple, red and black bars correspond to the intervals representing the LIA, the transition form the LIA to the MCA, the MCA, and the Dark Ages Cold Period respectively.
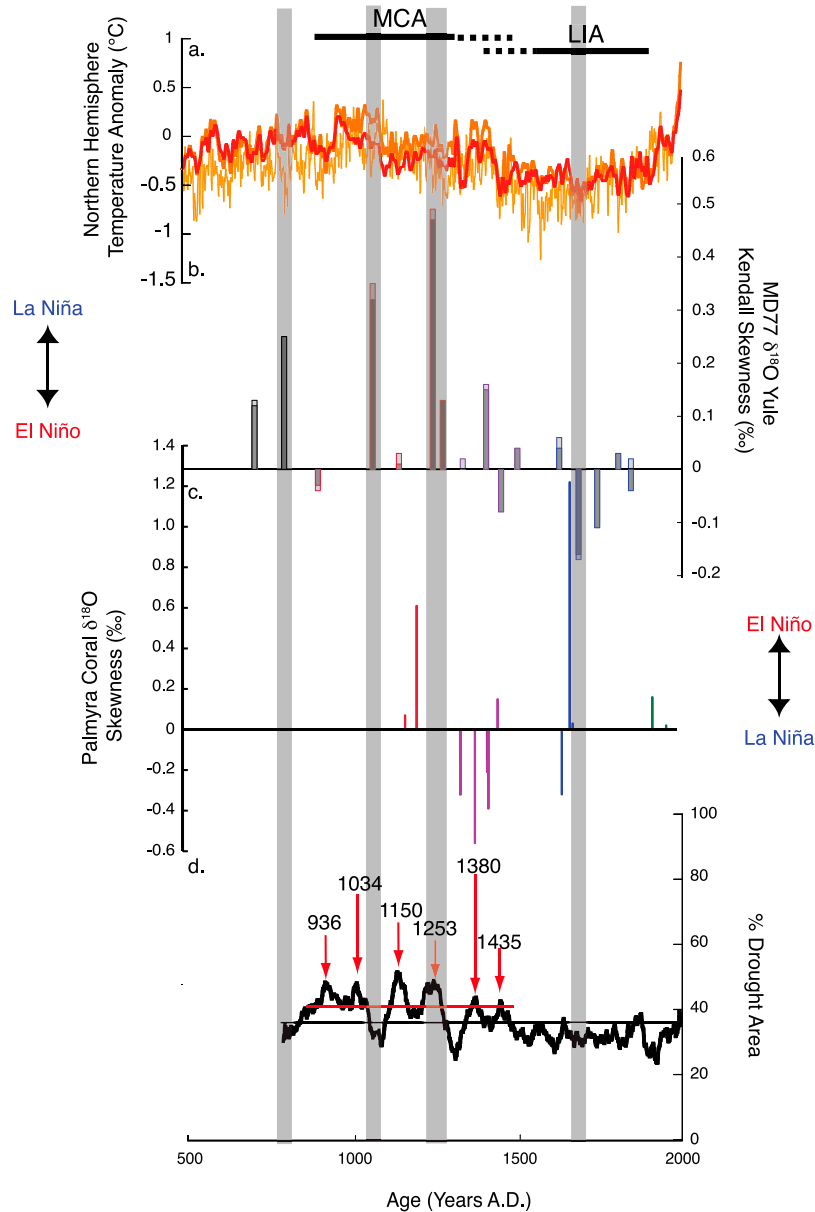
Figure 7. El Niño versus La Niña over the past millennium. (a) Northern Hemisphere temperature anomaly reconstructions from *Moberg et al.* [2005] (orange), and *Mann et al.* [2008] (land EIV temperature composite, dark orange, land + ocean EIV composite, red). (b) Yule Kendall Skewness values for each time slice sampled from MD98-2177. The light gray bars represent the YKS values for the entire data set. The dark gray bars represent the YKS values for the trimmed data set in which the highest and lowest $\delta^{18}O$ values were removed from the original data set. The statistics of the trimmed data set are not significantly different from that of the full distribution, which is consistent with the use of resistant statistics to quantify the moments of the distribution. The intervals with a significant skewness are highlighted in gray. In this record, the MCA is characterized by stronger/more frequent La Niña than El Niño. (c) Pearson's coefficient of skewness values for each time slice sampled from the Palmyra Island coral $\delta^{18}O$ record [*Cobb et al.*, 2003]. The blue, purple, red and black bars correspond to the intervals representing the LIA, the transition form the LIA to the MCA, the MCA, and the Dark Ages Cold Period respectively. (d) Drought area index (50-year smooth) for western North America over the past millennium [*Cook et al.*, 2004], with the long-term mean (horizontal black line). The arrows indicate the time of the medieval megadroughts [*Cook et al.*, 2004, 2007; *Herweijer et al.*, 2007; *Seager et al.*, 2008], which correspond within age uncertainty to stronger/more frequent La Niña events than El Niño in the MD77 and Palmyra record.

influencing the El Junco lake environment. Furthermore, an increase in the strength/frequency of both El Niño and La Niña events (with a larger increase in La Niña versus El Niño events to account for the skewness in the MD77 record) cannot explain this discrepancy in the El Junco records since this simultaneous increase would result in higher BSD/standard deviation values in the MD77 record or the Palmyra record, which are not observed (Figure 6).

[37] The Palmyra record also suggests that there were stronger/more frequent El Niño during the 17th century (Figure 7c), which corresponds within age model uncertainty to the interval 1681–1700 A.D. in our MD77 record. On the other hand, the YKS value for the LIA distributions is 0, which indicates that El Niño was not significantly stronger/more frequent than La Niña during that period. This discrepancy may be explained by our assumed increase in productivity in *P. obliquiloculata* during La Niña, which would bias the MD77 record against stronger/more frequent El Niño events.

6. Conclusions

[38] In this study we explored the use of $\delta^{18}O$ and $\delta^{13}C$ of individual *P. obliquiloculata* from marine sediment core MD98-2177 to investigate the history of ENSO variability during the past millennium. Changes in ENSO behavior was inferred from both the spread (BSD) and the symmetry (YKS) of individual $\delta^{18}O$ values of *P. obliquiloculata* from a sediment sample. Changes in the spread were used as a metric ENSO strength/frequency (i.e., simultaneous change in the strength/frequency of both El Niño and La Niña events) while the symmetry was interpreted in terms of the relative strength of El Niño and La Niña events. The main limitation of this proxy is the possibility that the depth habitat of *P. obliquiloculata* may change. This limitation was evaluated by comparing changes in the spread of the $\delta^{18}O$ values to those of the $\delta^{13}C$ values to distinguish between changes due to ENSO variability and varying habitat depth.

[39] Our results indicate that the strength/frequency of ENSO, as inferred from the spread of the $\delta^{18}O$ distributions, during the MCA and during the LIA was not statistically distinguishable and was comparable to that of the 20th century as inferred from the ECMWF-ORA S3 reanalysis data set. On the other hand, a coral record from the central Pacific [*Cobb et al.*, 2003] shows that the LIA was characterized by an increase in strength/frequency of ENSO events compared to the MCA or the 20th century. Both records document fairly large decadal changes in ENSO strength/frequency but smaller changes at centennial timescales. In our MD77 record, the MCA was also marked by an increase in the amplitude/frequency of La Niña events compared to El Niño (as evidenced by several positively skewed intervals in the MD77 record), in line with proxy evidence from the central and eastern tropical Pacific that suggests relatively cool conditions prevailed during this time period [*Cobb et al.*, 2003; *Conroy et al.*, 2009]. However, these results are in sharp contrast with the studies by *Moy et al.* [2002] and *Conroy et al.* [2008], which show an increase in the frequency of El Niño events during this time period. These periods of stronger La Niña as opposed to El Niño correspond within age model uncertainty to the time of medieval megadroughts in western North America

[*Cook et al.*, 2004, 2007]. These megadroughts have been hypothesized to be caused by an increase in the strength/frequency of La Niña events, a theory supported by our record.

References

An, S.-I., and F.-F. Jin (2004), Nonlinearity and asymmetry of ENSO, *J. Clim.*, *17*, 2399–2412, doi:10.1175/1520-0442(2004)017<2399: NAAOE>2.0.CO;2.

Anderson, R. Y. (1992), Long-term changes in the frequency of occurence of El Niño events, in *El Niño: Historical and Paleoclimatic Aspects of the Southern Oscillation*, edited by H. F. Diaz and V. Markgraf, pp. 193–200, Cambridge Univ. Press, Cambridge, U. K.

Ashok, K., and T. Yamagata (2009), The El Niño with a difference, *Nature*, *461*, 481–484, doi:10.1038/461481a.

Ashok, K., S. K. Behera, S. A. Rao, H. Weng, and T. Yamagata (2007), El Niño Modoki and its possible teleconnection, *J. Geophys. Res.*, *112*, C11007, doi:10.1029/2006JC003798.

Balmaseda, M. A., D. Dee, A. Vidard, and D. L. T. Anderson (2007), A multivariate treatment of bias for sequential data assimilation: Application to the tropical oceans, *Q. J. R. Meteorol. Soc.*, *133*, 167–179, doi:10.1002/qj.12.

Balmaseda, M. A., A. Vidard, and D. L. T. Anderson (2008), The ECMWF Ocean Analysis System: ORA-S3, Mon. *Weather Rev.*, *136*, 3018–3034, doi:10.1175/2008MWR2433.1.

Barker, S., M. Greaves, and H. Elderfield (2003), A study of cleaning procedures used for foraminiferal Mg/Ca paleothermometry, *Geochem. Geophys. Geosyst.*, *4*(9), 8407, doi:10.1029/2003GC000559.

Bell, M. J., M. J. Martin, and N. K. Nichols (2004), Assimilation of data into an ocean model with systematics errors near the equator, *Q. J. R. Meteorol. Soc.*, *130*, 873–893, doi:10.1256/qj.02.109.

Bemis, B. E., H. J. Spero, J. Bijma, and D. W. Lea (1998), Reevaluation of the oxygen isotopic composition of planktonic foraminifera: Experimental results and revised paleotemperature equations, *Paleoceanography*, *13*, 150–160, doi:10.1029/98PA00070.

Benway, H. M., and A. C. Mix (2004), Oxygen isotopes, upper-ocean salinity, and precipitation sources in the eastern tropical Pacific, *Earth Planet. Sci. Lett.*, *224*, 493–507, doi:10.1016/j.epsl.2004.05.014.

Bowley, A. L. (1920), *Elements of statistics*, Scribner, New York.

Bray, N. A., S. Hautala, J. Chong, and J. Pariwono (1996), Large-scale sea level, thermocline, and wind variations in the Indonesian throughflow region, *J. Geophys. Res.*, *101*, 12,239–12,254, doi:10.1029/96JC00080.

Brown, M. B., and A. B. Forsythe (1974), Robust tests for the equality of variances, *J. Am. Stat. Assoc.*, *69*(346), 364–367, doi:10.2307/2285659.

Burgers, G., and D. B. Stephenson (1999), The "normality" of El Niño, *Geophys. Res. Lett.*, *26*, 1027–1030, doi:10.1029/1999GL900161.

Burgman, R., R. Seager, A. Clement, and C. Herweijer (2010), The role of tropical Pacific SSTs in global medieval hydroclimate: A modeling study, *Geophys. Res. Lett.*, *37*, L06705, doi:10.1029/2009GL042239.

Cléroux, C., E. Cortijo, J. C. Duplessy, and R. Zahn (2007), Deep-dwelling foraminifera as thermocline temperature recorders, *Geochem. Geophys. Geosyst.*, *8*, Q04N11, doi:10.1029/2006GC001474.

Cobb, K. M., C. D. Charles, H. Cheng, and R. L. Edwards (2003), El Niño/Southern Oscillation and tropical Pacific climate during the last millennium, *Nature*, *424*, 271–276, doi:10.1038/nature01779.

Conroy, J. L., J. T. Overpeck, J. E. Cole, T. M. Shanahan, and M. Steinitz-Kannan (2008), Holocene changes in eastern tropical Pacific climate inferred from a Galapagos lake sediment record, *Quat. Sci. Rev.*, *27*, 1166–1180, doi:10.1016/j.quascirev.2008.02.015.

Conroy, J. L., A. Restrepo, J. T. Overpeck, M. Steinitz-Kannan, J. E. Cole, M. B. Bush, and P. A. Colinvaux (2009), Unprecendented recent warming of surface temperatures in the eastern tropical Pacific Ocean, *Nat. Geosci.*, *2*, 46–50, doi:10.1038/ngeo390.

Conroy, J. L., J. T. Overpeck, and J. E. Cole (2010), El Niño/Southern Oscillation and changes in the zonal gradient of tropical Pacific sea surface temperature over the last 1.2ka, *PAGES News*, *18*(1), 32–34.

Cook, E. R., C. A. Woodhouse, C. M. Eakin, D. M. Meko, and D. W. Stahle (2004), Long-term aridity changes in the Western United States, *Science*, *306*, 1015–1018, doi:10.1126/science.1102586.

Cook, E. R., R. Seager, M. A. Cane, and D. W. Stahle (2007), North American drought: Reconstructions, causes, and consequences, *Earth Sci. Rev.*, *81*, 93–134, doi:10.1016/j.earscirev.2006.12.002.

Dunbar, R. B., G. M. Wellington, M. W. Colgan, and P. W. Glynn (1994), Eastern Pacific sea surface temperature since 1600 A.D.: The $\delta^{18}O$ record of climate variability in the Galapagos corals, *Paleoceanography*, *9*, 291–315, doi:10.1029/93PA03501.

England, M. H., and F. Huang (2005), On the interannual varaibility of the Indoensian Throughflow and its linkage with ENSO, *J. Clim.*, *18*, 1435–1444, doi:10.1175/JCLI3322.1.

Erez, J., and S. Honjo (1981), Comparison of isotopic composition of planktonic foraminifera in plankton tows, sediment traps and sediments, *Palaeogeogr. Palaeoclimatol. Palaeoecol.*, *33*, 129–156, doi:10.1016/0031-0182(81)90035-3.

Fairbanks, R. G., M. N. Evans, J. L. Rubenstone, R. A. Mortlock, K. Broad, M. D. Moore, and C. D. Charles (1997), Evaluating climate indices and their geochemical proxies measured in corals, *Coral Reefs*, *16*, S93–S100, doi:10.1007/s003380050245.

Ffield, A., K. Vranes, A. L. Gordon, and R. D. Susanto (2000), Temperature variability within Makassar Strait, *Geophys. Res. Lett.*, *27*, 237–240, doi:10.1029/1999GL002377.

Fieux, M., R. Molcard, and A. G. Ilahude (1996), Geostrophic transport of the Pacific-Indian Oceans throughflow, *J. Geophys. Res.*, *101*, 12,421–12,432, doi:10.1029/95JC03566.

Gordon, A. L. (1986), Interocean exchange of thermocline water, *J. Geophys. Res.*, *91*, 5037–5046, doi:10.1029/JC091iC04p05037.

Gordon, A. L. (2005), Oceanography of the Indonesian Seas and their throughflow, *Oceanography*, *18*(4), 14–27.

Gordon, A. L., and R. A. Fine (1996), Pathways of water between the Pacific and Indian Oceans in the Indonesian Seas, *Nature*, *379*, 146–149, doi:10.1038/379146a0.

Gordon, A. L., and R. D. Susanto (1999), Makassar Strait transport: Initial estimate based on Arlindo results, *Mar. Technol. Soc. J.*, *32*, 34–45.

Gordon, A. L., R. D. Susanto, and A. Ffield (1999), Throughflow within Makassar Strait, *Geophys. Res. Lett.*, *26*, 3325–3328, doi:10.1029/1999GL002340.

Gordon, A. L., R. D. Susanto, and K. Vranes (2003), Cool Indonesian throughflow as a consequence of restricted surface layer flow, *Nature*, *425*, 824–828, doi:10.1038/nature02038.

Gordon, A. L., R. D. Susanto, A. Ffield, B. A. Huber, W. Pranowo, and S. Wirasantosa (2008), Makassar Strait throughflow, 2004 to 2006, *Geophys. Res. Lett.*, *35*, L24605, doi:10.1029/2008GL036372.

Guilyardi, E., A. T. Wittenberg, A. Fedorov, M. Collins, C. Wang, A. Capotondi, G. J. van Oldenborgh, and T. Stockdale (2009), Understanding El Niño in ocean-atmosphere general circulation models: Progress and challenges, *Bull. Am. Meteorol. Soc.*, *90*, 325, doi:10.1175/2008BAMS2387.1.

Hannachi, A., D. B. Stepgenson, and K. R. Sperber (2003), Probability-based methids for quantifying nonlinearity in the ENSO, *Clim. Dyn.*, *20*, 241–256.

Hemleben, C., M. Spindler, and O. R. Anderson (1989), *Modern Planktonic Foraminifera*, Springer, Berlin.

Hendon, H. H., E. Lim, G. Wang, O. Alves, and D. Hudson (2009), Prospects for predicting two flavors of El Niño, *Geophys. Res. Lett.*, *36*, L19713, doi:10.1029/2009GL040100.

Hereid, K. A., T. M. Quinn, F. W. Taylor, and J. Banner (2009), Interannual to multi-decadal scale climate variability in the Western Pacific Warm Pool recorded by the geochemistry of 16–17th century corals from Papua New Guinea, *EOS Trans. AGU*, *90*(52), Fall Meet. Suppl., Abstract PP11G-04.

Herweijer, C., R. Seager, E. R. Cook, and J. Emile-Geay (2007), North American droughts of the last millennium fron a gridded network of tree-ring data, *J. Clim.*, *20*(7), 1353–1376, doi:10.1175/JCLI4042.1.

Hoaglin, D., F. Mosteller, and J. Tukey (1983), *Understanding Robust and Exploratory Data Analysis*, 447 pp., Wiley, New York.

Jin, F.-F., S.-I. An, A. Timmermman, and J. Zhao (2003), Strong El Niño events and nonlinear dynamical heating, *Geophys. Res. Lett.*, *30*(3), 1120, doi:10.1029/2002GL016356.

Jones, P. D., and M. E. Mann (2004), Climate over past millennia, *Rev. Geophys.*, *42*, RG2002, doi:10.1029/2003RG000143.

Kao, H.-Y., and J.-Y. Yu (2009), Contrasting Eastern-Pacific and Central-Pacific types of ENSO, *J. Clim.*, *22*, 615–632, doi:10.1175/2008JCLI2309.1.

Kim, H.-M., P. J. Webster, and J. A. Curry (2009), Impact of shifting patterns of Pacific Ocean warming on North Atlantic tropical cyclones, *Science*, *325*, 77–80, doi:10.1126/science.1174062.

Kinkade, C., J. Marra, C. Langdon, C. Knudson, and A. G. Gani Ilahude (1997), Monsoonal differences in phytoplankton biomass and production in the Indoensian Seas: Tracing vertical mixing using temperature, *Deep Sea Res.*, Part I, *44*, 581–592, doi:10.1016/S0967-0637(97)00002-2.

Koutavas, A., P. B. deMenocal, G. C. Olive, and J. Lynch-Stieglitz (2006), Mid-Holocene El Nino-Southern Oscillation (ENSO) attenuation revealed by individual foraminifera in eastern tropical Pacific sediments, *Geology*, *34*, 993–996, doi:10.1130/G22810A.1.

Kug, J.-S., F.-F. Jin, and S.-I. An (2009), Two types of El Niño events: Cold tongue El Niño and Warm Pool El Niño, *J. Clim.*, *22*, 1499–1515, doi:10.1175/2008JCLI2624.1.

Kumar, K. K., B. Rajagopalan, M. Hoerling, G. Bates, and M. Cane (2006), Unraveling the mystery of Indian Monsoon failure during El Niño, *Science*, *314*, 115–119, doi:10.1126/science.1131152.

Lanzante, J. R. (1996), Resistant, robust and non-paramtric techniques for the analysis of climate data: Theory and examples, including applications to historical radiosonde station data, *Int. J. Climatol.*, *16*, 1197–1226, doi:10.1002/(SICI)1097-0088(199611)16:11<1197::AID-JOC89>3.0.CO;2-L.

Larkin, N. K., and D. E. Harrison (2005a), Global seasonal temperature and precipitation anomalies during El Niño autumn and winter, *Geophys. Res. Lett.*, *32*, L16705, doi:10.1029/2005GL022860.

Larkin, N. K., and D. E. Harrison (2005b), On the definition of El Niño and associated seasonal average U.S. weather anomalies, *Geophys. Res. Lett.*, *32*, L13705, doi:10.1029/2005GL022738.

Lau, K. M., and H. Weng (1999), Interannual, decadal-interdecadal, and global warming signals in sea surface temperature during 1955–97, *J. Clim.*, *12*, 1257–1267, doi:10.1175/1520-0442(1999)012<1257:IDIAGW>2.0.CO;2.

Leduc, G., L. Vidal, O. Cartapanis, and E. Bard (2009), Modes of eastern equatorial Pacific thermocline variability: Implications for ENSO dynamics over the last glacial period, *Paleoceanography*, *24*, PA3202, doi:10.1029/2008PA001701.

LeGrande, A. N., and G. A. Schmidt (2006), Global gridded data set of the oxygen isotopic composition in seawater, *Geophys. Res. Lett.*, *33*, L12604, doi:10.1029/2006GL026011.

Lim, E.-P., H. H. Hendon, D. Hudson, G. Wang, and O. Alves (2009), Dynamical forecasts of inter-El Niño variations of tropical SST and Australian spring rainfall, *Mon. Weather Rev.*, *137*, 3796–3810, doi:10.1175/2009MWR2904.1.

Mann, M. E., Z. Zhang, M. K. Hughes, R. S. Bradley, S. K. Miller, S. Rutherford, and F. Ni (2008), Proxy-based reconstructions of hemispheric and global surface temperature variations over the past two millennia, *Proc. Natl. Acad. Sci. U. S. A.*, *105*(36), 13,252–13,257, doi:10.1073/pnas.0805721105.

Meehl, G. A., et al. (2007), Global climate projections, in *Climate Change 2007: The Physical Science Basis. Contribution of Working Group I to the Fourth Assessment Report of the Intergovernmental Panel on Climate Change*, edited by S. Solomon et al., pp. 747–845, Cambridge Univ. Press, Cambridge, U. K.

Meyers, G. (1996), Variation of Indonesian throughflow and the El Niño–Southern Oscillation, *J. Geophys. Res.*, *101*(C5), 12,255–12,263, doi:10.1029/95JC03729.

Moberg, A., D. M. Sonechkin, K. Holmgren, N. M. Datsenko, and W. Karlen (2005), Highly variable Northern Hemisphere temperatures reconstructed from low- and high-resolution proxy data, *Nature*, *433*, 613–617, doi:10.1038/nature03265.

Mohtadi, M., S. Steinke, J. Groeneveld, H. G. Fink, T. Rixen, D. Hebbeln, B. Donner, and B. Herunadi (2009), Low-latitude control on seasonal and interannual changes in planktonic foraminiferal flux and shell geochemistry off south Java: A sediment trap study, *Paleoceanography*, *24*, PA1201, doi:10.1029/2008PA001636.

Monahan, A. H., and A. Dai (2004), The spatial and temporal structure of ENSO nonlinearity, *J. Clim.*, *17*, 3026–3036, doi:10.1175/1520-0442(2004)017<3026:TSATSO>2.0.CO;2.

Morimoto, M., O. Abe, H. Kayanne, N. Kurita, E. Matsumoto, and N. Yoshida (2002), Salinity records for the 1997–98 El Nino from Western Pacific corals, *Geophys. Res. Lett.*, *29*(11), 1540, doi:10.1029/2001GL013521.

Moy, C. M., G. O. Seltzer, D. T. Rodbell, and D. M. Anderson (2002), Variability of El Niño/Southern Oscillation activity at millennial timescales during the Holocene epoch, *Nature*, *420*, 162–165, doi:10.1038/nature01194.

Mulitza, S., H. Arz, S. Kemle-von Mucke, C. Moos, H.-S. Niebler, J. Pätzold, and M. Segl (1999), The south Atlantic carbon isotope record of planktic foraminifera, in *Use of Proxies in Paleoceanography: Examples From the South Atlantic*, edited by G. Fischer and G. Wefer, pp. 427–445, Springer, Berlin.

Oppo, D. W., Y. Rosenthal, and B. K. Linsley (2009), 2,000-year-long temperature and hydrology reconstructions from the Indo-Pacific warm pool, *Nature*, *460*, 1113–1116, doi:10.1038/nature08233.

Qu, T., Y. Du, J. Strachan, G. Meyers, and J. Slingo (2005), Sea surface temperature and its variability in the Indonesian region, *Oceanography*, *18*(4), 50–61.

Quinn, T. M., F. W. Taylor, and T. J. Crowley (2006), Coral-based climate variability in the western Pacific warm pool, *J. Geophys. Res.*, *111*, C11006, doi:10.1029/2005JC003243.

Quinn, W. H. (1992), A study of Southern Oscillation-related climatic activity for A.D. 622–1990 incorporating Nile River flood data, in *El Nino: Historical and Paleoclimatic Aspects of the Southern Oscillation*, edited by H. F. Diaz and V. Markgraf, pp. 119–149, Cambridge Univ. Press, Cambridge, U. K.

Rasmusson, E. M., and T. H. Carpenter (1982), Variations in tropical sea surface temperatures and surface wind fields associated with the Southern Oscillation/El Niño, *Mon. Weather Rev.*, *110*, 354–384, doi:10.1175/1520-0493(1982)110<0354:VITSST>2.0.CO;2.

Ravelo, A. C., and R. G. Fairbanks (1992), Oxygen istopic composition of multiple species of planktonic foraminifera: Recorders of the modern photic zone temperature gradient, *Paleoceanography*, *7*, 815–831, doi:10.1029/92PA02092.

Rayner, N. A., D. E. Parker, E. B. Horton, C. K. Folland, L. V. Alexander, D. P. Rowell, E. C. Kent, and A. Kaplan (2003), Global analyses of sea surface temperature, sea ice and night marine air temperature since the late nineteenth century, *J. Geophys. Res.*, *108*(D14), 4407, doi:10.1029/2002JD002670.

Russell, A. D., and H. J. Spero (2000), Field examination of the oceanic carbonate ion effect on stable isotopes in planktonic foraminifera, *Paleoceanography*, *15*, 43–52, doi:10.1029/1998PA000312.

Seager, R., R. Burgman, Y. Kushnir, A. Clement, E. Cook, N. Naik, and J. Velez (2008), Tropical Pacific forcing of North American Medieval megadroughts: Testing the concept with an atmosphere model forced by coral-reconstructed SSTs, *J. Clim.*, *21*, 6175–6190, doi:10.1175/2008JCLI2170.1.

Southon, J., M. Kashgarian, M. R. Fontugne, B. Metivier, and W. W.-S. Yim (2002), Marine reservoir corrections for the Indian ocean and southeast Asia, *Radiocarbon*, *44*, 167–180.

Spero, H. J. (1998), Life history and stable isotope geochemistry of planktonic foraminifera, in *Isotope Pakeobiology and Paleoecology*, edited by R. D. Norris and R. M. Corfield, pp. 7–36, Paleontol. Soc. Pap., Pittsburg, Penn.

Sprintall, J. (2009), Indonesian Throughflow, in *Encyclopedia of Ocean Sciences*, edited by J. H. Steele, K. K. Turekian, and S. A. Thorpe, pp. 237–243, Elsevier, Boston, Mass., doi:10.1016/B978-012374473-9.00602-0.

Stott, L. D., and C. M. Tang (1996), Reassessment of tropical sea surface δ^{18}O paleotemperatures, *Paleoceanography*, *11*, 37–56, doi:10.1029/95PA03344.

Stuiver, M., and P. J. Reimer (1993), Extended ^{14}C data base and revised CALIB 3.0 ^{14}C age calibration program, *Radiocarbon*, *35*, 215–230.

Susanto, R. D., and A. L. Gordon (2005), Velocity and transport of the Makassar Strait throughflow, *J. Geophys. Res.*, *110*, C01005, doi:10.1029/2004JC002425.

Tang, C. M., and L. D. Stott (1993), Seasonal salinity changes during Mediterranean sapropel deposition 9,000 years B.P.: Evidence from isotopic analyses of individual planktonic foraminifera, *Paleoceanography*, *8*, 473–494, doi:10.1029/93PA01319.

Thompson, L. G., E. Mosley-Thompson, and B. Morales Arnao (1984), El Niño-Southern Oscillation events recorded in the stratigraphy of the tropical Quelccaya ice cap, Peru, *Science*, *226*, 50–53, doi:10.1126/science.226.4670.50.

Tomascik, T., A. J. Mah, A. Nontji, and M. K. Moosa (1997), *The Ecology of the Indonesian Seas*, 642 pp., Periplus Ed., Singapore.

Trenberth, K. E. (1997), The definition of El Niño, *Bull. Am. Meteorol. Soc.*, *78*, 2771–2777, doi:10.1175/1520-0477(1997)078<2771:TDOENO>2.0.CO;2.

Trenberth, K. E., and D. P. Stepaniak (2001), Indices of El Niño evolution, *J. Clim.*, *14*, 1697–1701, doi:10.1175/1520-0442(2001)014<1697:LIOENO>2.0.CO;2.

Wang, G., and H. H. Hendon (2007), Sensitivity of Australian rainfall to inter-El Niño variations, *J. Clim.*, *20*, 4211–4226, doi:10.1175/JCLI4228.1.

Watkins, J. M., A. C. Mix, and J. Wilson (1996), Living planktonic foraminifera: Tracers of circulation and productivity in the central equatorial Pacific, *Deep Sea Res.*, *Part II*, *43*, 1257–1282, doi:10.1016/0967-0645(96)00008-2.

Wejnert, K. E., C. J. Pride, and R. C. Thunell (2010), The oxygen isotope composition of planktonic foraminifera from the Guaymas Basin, Gulf of California: Seasonal, annual, and interspecies variability, *Mar. Micropaleontol.*, *74*, 29–37, doi:10.1016/j.marmicro.2009.11.002.

Weng, H., K. Ashok, S. K. Behera, S. A. Rao, and T. Yamagata (2007), Impacts of recent El Niño Modoki on dry/wet conditions in the Pacific rim during boreal summer, *Clim. Dyn.*, *29*, 113–129, doi:10.1007/s00382-007-0234-0.

Weng, H., S. K. Behera, and T. Yamagata (2009), Anomalous winter climate conditions in the Pacific rim during recent El Niño Modoki and El Niño events, *Clim. Dyn.*, *32*, 663–674, doi:10.1007/s00382-008-0394-6.

Xu, J., A. Holbourn, W. Kuhnt, Z. Jian, and H. Kawamura (2008), Changes in the thermocline structure of the Indonesia outflow during Terminations I and II, *Earth Planet. Sci. Lett.*, *273*, 152–162, doi:10.1016/j.epsl.2008.06.029.

Yeh, S.-W., J.-S. Kug, B. Dewitte, M.-H. Kwon, B. P. Kirtman, and F.-F. Jin (2009), El Niño in a changing climate, *Nature*, *461*, 511–514, doi:10.1038/nature08316.

Yu, J.-Y., H.-Y. Kao, T. Lee, and S. T. Kim (2011), Subsurface ocean temperature indices for Central-Pacific and Eastern-Pacific types of El Niño and La Niña events, *Theor. Appl. Climatol.*, *103*, 337–344, doi:10.1007/s00704-010-0307-6.

J. Emile-Geay, D. E. Hammond, D. Khider, and L. D. Stott, Department of Earth Science, University of Southern California, 3651 Trousdale Pkwy., Los Angeles, CA 90089, USA. (khider@usc.edu)

R. Thunell, Department of Earth and Ocean Sciences, University of South Carolina, 701 Sumter St., EWSC Rm. 617, Columbia, SC 29208, USA.